J. Fluid Mech. (2009), *vol.* 631, *pp.* 165–197.
doi:10.1017/S0022112009007010 Printed in the United Kingdom

Dynamics of ultra-thin two-layer films under the action of inclined temperature gradients

ALEXANDER A. NEPOMNYASHCHY[1, 2] AND ILYA B. SIMANOVSKII[1,2]†

[1]Department of Mathematics, Technion – Israel Institute of Technology, 32000, Haifa, Israel

[2]Minerva Centre for Nonlinear Physics of Complex Systems, Technion – Israel Institute of Technology, 32000, Haifa, Israel

(Received 15 January 2008 and in revised form 26 February 2009)

The development of instabilities under the joint action of the van der Waals forces and Marangoni stresses in a two-layer film in the presence of an inclined temperature gradient is investigated. The problem is solved by means of a linear stability theory and nonlinear simulations. It has been found that for sufficiently large values of the ratio between the longitudinal and transverse Marangoni numbers, the real part of the linear growth rate does not depend on the direction of the wavenumber, except the case of nearly longitudinal disturbances. Numerous types of nonlinear evolution have been observed, among them are ordered systems of droplets, 'splashes', oblique waves, modulated transverse and longitudinal structures.

1. Introduction

Two-layer fluid systems are widespread in nature and engineering. When the layers are sufficiently thin, the flows are strongly affected by interfacial phenomena, specifically by the Marangoni effect. Marangoni convection in two-layer fluid systems has been studied both in the case of a temperature gradient applied across the layers and in the case of a temperature gradient directed along the interfaces, as well as for a temperature gradient inclined with respect to the interface (Simanovskii & Nepomnyashchy 1993; Nepomnyashchy, Simanovskii & Legros 2006). The latter case is of a special interest. The interplay between the thermocapillary flow generated by the longitudinal component of the temperature gradient and the Marangoni instability caused by the transverse component of the temperature gradient can lead to qualitatively new phenomena. Until now, Marangoni convection under the action of inclined temperature gradients has been studied only for relatively thick layers where the instability of a thermocapillary flow manifests itself in the form of hydrothermal waves or convection patterns, while the deformations of the interfaces are not important (Davis 1987; Nepomnyashchy, Simanovskii & Braverman 2001; Ueno, Kurosawa & Kawamura 2002; Ospennikov & Schwabe 2004; Shklyaev & Nepomnyashchy 2004; Simanovskii *et al.* 2006).

In the past few decades, the development of microfluidics and nanotechnology led to significant progress in the exploration of thin film flows. Such kinds of flows

† Email address for correspondence: yuri11@inter.net.il

have numerous technological applications (coating, flotation, biological membranes, adhesives etc.). The instabilities in thin films are of potential use in the formation of regular nanostructures and ordered porous membranes, in soft lithographic techniques and in other areas of nanotechnology.

The dynamics of ultra-thin (but still macroscopic) films, with the thickness less than 100 nm, is of great importance. In the case of ultra-thin films, it is necessary to take into account the long-range intermolecular forces (first of all, van der Waals forces) acting between molecules of the liquid and substrate (Israelachvili 1992). Depending on the sign of the Hamaker constant, these forces can either stabilize the film or create a longwave instability leading to the film rupture through the formation of holes (Oron, Davis & Bankof 1997).

The dynamics of multilayer ultra-thin films is characterized by several Hamaker constants, which can be of different signs, therefore it can be much richer. A theoretical description of instabilities in two-layer systems sandwiched between two solid plates has been developed by Joo & Hsieh (2000), Merkt *et al.* (2005) and Lenz & Kumar (2007*a*). Two-layer systems that include a bottom layer resting on a solid substrate and a top layer in contact with a gas phase have been studied by Pototsky *et al.* (2004, 2005, 2006), Bandyopadhyay, Gulabani & Sharma (2005), Fisher & Golovin (2005), Bandyopadhyay & Sharma (2006) and Bandyopadhyay, Sharma & Rastogi (2008). A three-layer film confined between solid walls has been studied by Lenz & Kumar (2007*b*). Instabilities of ultra-thin two-layer films caused by intermolecular forces have been observed in experiments by Faldi, Composto & Winey (1995), Lambooy *et al.* (1996), Pan *et al.* (1997), Sferrazza *et al.* (1997, 1998), David *et al.* (1998), Renger *et al.* (2000) and Morariu, Schaffer & Steiner (2003).

The dynamics of ultra-thin films under the joint action of the Marangoni effect and van der Waals forces has not yet been extensively explored. The authors are not aware of any experimental works on that subject. Merkt *et al.* (2005) and Pototsky *et al.* (2005) have considered a general structure of the evolution equations. The development of instabilities has been studied either in the case of a temperature gradient directed along the interfaces (Miladinova *et al.* 2002; Nepomnyashchy & Simanovskii 2006) or in the case of a temperature gradient applied across the layers (Joo & Hsieh 2000; Nepomnyashchy & Simanovskii 2007). It is reasonable to consider the situation when the temperature gradient is inclined with respect to the interfaces also for ultra-thin films. Let us emphasize that the instability mechanisms in thin films are completely different from those in thick layers. The instabilities which are developed due to van der Waals forces and Marangoni stresses lead to significant deformations of the interfaces. The subject of the present paper is the development of deformational instabilities in a thin two-layer film under the action of an inclined temperature gradient. To our knowledge, the latter kind of instabilities has never been studied formerly for ultra-thin films, neither theoretically nor experimentally.

The mathematical model is formulated in § 2. The linear stability of a parallel thermocapillary flow is considered in § 3. It is shown that in thin layers, in contradistinction to the results obtained for thick layers, a novel effect, isotropization of the growth rate dependence on the wavevector for three-dimensional disturbances, takes place. Section 4 is devoted to numerical simulations of the nonlinear problem. A new phenomenon, formation of regular structures, is observed: droplets created in the course of the film decomposition due to the action of van der Waals forces can be ordered by the thermocapillary flow. A summary of results is given in § 5.

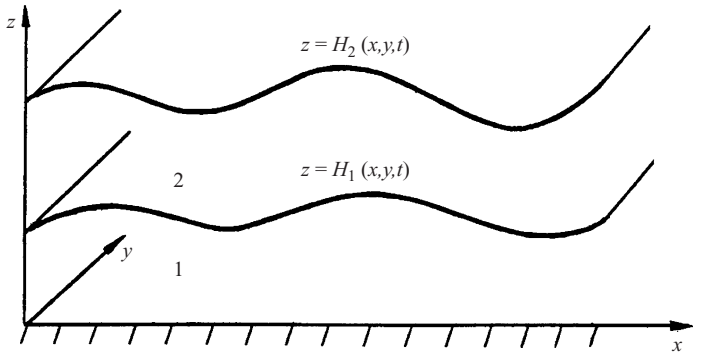

FIGURE 1. Geometric configuration of the region and coordinate axes

2. Long-wave evolution equations

2.1. *Thermocapillary flow*

2.1.1. *Formulation of the problem*

Consider a system of two superposed layers of immiscible liquids with different physical properties (see figure 1). The bottom layer rests on a solid substrate, while the top layer is in contact with the adjacent gas phase. The temperature of the solid substrate is $T_s + Ax$, and the temperature of the gas near the interface is $T_g + Ax$. Thus, it is assumed that the same constant temperature gradient is imposed in the direction of the axis x in the solid substrate and in the gas phase. All the variables referring to the bottom layer are marked by subscript 1, and all the variables referring to the top layer are marked by subscript 2. The equilibrium thicknesses of the layers are H_i^0, $i = 1, 2$. The deformable interfaces are described by equations $z = H_1(x, y, t)$ (liquid–liquid interface) and $z = H_2(x, y, t)$ (liquid–gas interface). The ith fluid has density ρ_i, kinematic viscosity ν_i, dynamic viscosity $\eta_i = \rho_i \nu_i$, thermal diffusivity χ_i and heat conductivity κ_i. The surface tension coefficients on the lower and upper interfaces, σ_1 and σ_2, are linear functions of temperature T: $\sigma_1 = \sigma_1^0 - \alpha_1 T$, $\sigma_2 = \sigma_2^0 - \alpha_2 T$. The effect of gravity is neglected. The intermolecular forces are neglected in this subsection.

The complete system of nonlinear equations governing Marangoni convection is written in the following form (Simanovskii & Nepomnyashchy 1993):

$$\frac{\partial \boldsymbol{v}_m}{\partial t} + (\boldsymbol{v}_m \cdot \nabla)\boldsymbol{v}_m = -\frac{1}{\rho_m}\nabla P_m + \nu_m \Delta \boldsymbol{v}_m, \tag{2.1}$$

$$\frac{\partial T_m}{\partial t} + \boldsymbol{v}_m \cdot \nabla T_m = \chi_m \Delta T_m, \tag{2.2}$$

$$\nabla \cdot \boldsymbol{v}_m = 0, \ \ m = 1, 2. \tag{2.3}$$

Here, $\boldsymbol{v}_m$ and P_m are the velocity and the difference between the overall pressure and the atmospheric pressure in the mth liquid, correspondingly. The boundary conditions on the rigid boundary are:

$$\boldsymbol{v}_1 = 0, \ T_1 = T_s + Ax, \ \text{at} \ \ z = 0. \tag{2.4}$$

On the deformable interface $z = H_1$, the following boundary conditions hold: the balance of normal stresses

$$P_2 - P_1 + 2\sigma_1 K_1 = \left[-\eta_1\left(\frac{\partial v_{1i}}{\partial x_k} + \frac{\partial v_{1k}}{\partial x_i}\right) + \eta_2\left(\frac{\partial v_{2i}}{\partial x_k} + \frac{\partial v_{2k}}{\partial x_i}\right)\right] n_{1i} n_{1k}; \ i, k = 1, 2, 3; \tag{2.5}$$

the balance of tangential stresses

$$\left[-\eta_1\left(\frac{\partial v_{1i}}{\partial x_k}+\frac{\partial v_{1k}}{\partial x_i}\right)+\eta_2\left(\frac{\partial v_{2i}}{\partial x_k}+\frac{\partial v_{2k}}{\partial x_i}\right)\right]\tau_{1i}^{(l)}n_{1k}-\alpha_1\tau_{1i}^{(l)}\frac{\partial T_1}{\partial x_i}=0,$$
$$l=1,2;i,k=1,2,3; \quad (2.6)$$

the continuity of the velocity field

$$\boldsymbol{v}_1=\boldsymbol{v}_2; \quad (2.7)$$

the kinematic equation for the interface motion

$$\frac{\partial H_1}{\partial t}+v_{1x}\frac{\partial H_1}{\partial x}+v_{1y}\frac{\partial H_1}{\partial y}=v_{1z}; \quad (2.8)$$

the continuity of the temperature field

$$T_1=T_2; \quad (2.9)$$

and the balance of normal heat fluxes

$$\left(\kappa_1\frac{\partial T_1}{\partial x_i}-\kappa_2\frac{\partial T_2}{\partial x_i}\right)n_{1i}=0. \quad (2.10)$$

Similar boundary conditions are imposed on the deformable interface $z=H_2$:

$$-P_2+2\sigma_2K_2=-\eta_2\left(\frac{\partial v_{2i}}{\partial x_k}+\frac{\partial v_{2k}}{\partial x_i}\right)n_{2i}n_{2k}, \quad (2.11)$$

$$-\eta_2\left(\frac{\partial v_{2i}}{\partial x_k}+\frac{\partial v_{2k}}{\partial x_i}\right)\tau_{2i}^{(l)}n_{2k}-\alpha_2\tau_{2i}^{(l)}\frac{\partial T_3}{\partial x_i}=0,\ l=1,2,\ i,k=1,2,3, \quad (2.12)$$

$$\frac{\partial H_2}{\partial t}+v_{2x}\frac{\partial H_2}{\partial x}+v_{2y}\frac{\partial H_2}{\partial y}=v_{2z}, \quad (2.13)$$

where K_1 and K_2 are the mean curvatures, $\boldsymbol{n}_1$ and $\boldsymbol{n}_2$ are the normal vectors and $\boldsymbol{\tau}_1^{(l)}$ and $\boldsymbol{\tau}_2^{(l)}$ are the tangential vectors of the lower and upper interfaces. In the quantities with two subscripts, the first subscript corresponds to the number of the liquid ($m=1,2$) and the second subscript determines the number of the Cartesian coordinate ($i,k=1,2,3$; $x_1=x$, $x_2=y$, $x_3=z$). The usual summation convention is applied. For a heat flux on the liquid–gas interface, we use an empirical condition

$$\kappa_2\frac{\partial T_2}{\partial x_i}n_{2i}=-q(T_2-T_g-Ax), \quad (2.14)$$

where q is the heat exchange coefficient which is assumed to be constant.

2.1.2. *Derivation of the longwave amplitude equation*

The system of equations and boundary conditions (2.1)–(2.14) is rather complicated. However, in the case of thin film flows, when the fluid system is thin in one direction and extended in other directions, the nonlinear model governing three-dimensional flows with a deformable interface can be drastically simplified by means of a *long-wavelength expansion*. The leading order of this expansion is known as *the lubrication approximation*. The longwave approach is based on the assumption that the characteristic spatial scales in the directions x and y are much larger than that in the direction z. It is assumed that the solution of equations and boundary conditions (2.1)–(2.14) depends on the scaled horizontal coordinates $X=\epsilon x$ and $Y=\epsilon y$, $\epsilon\ll 1$,

rather than on x and y. Also, it is assumed that the solution depends on the scaled time variable $\tau = \epsilon t$. The details of the longwave approach applied to thermocapillary flows can be found in review papers (Davis 1987; Oron *et al.* 1997).

At the leading order, the evolution of the system is governed by the following equations and boundary conditions:

$$U_{1zz} = 0;\ V_{1zz} = 0;\ U_{1X} + V_{1Y} + W_{1z} = 0;\ T_{1zz} = 0;\ 0 < z < H_1; \tag{2.15}$$

$$U_{2zz} = 0;\ V_{2zz} = 0;\ U_{2X} + V_{2Y} + W_{2z} = 0;\ T_{2zz} = 0;\ H_1 < z < H_2; \tag{2.16}$$

$$z = 0:\ U_1 = V_1 = W_1 = 0;\ T_1 = T_s + Ax; \tag{2.17}$$

$$z = H_1:\ U_1 = U_2;\ V_1 = V_2;\ W_1 = W_2; \tag{2.18}$$

$$\eta_2 U_{2z} - \eta_1 U_{1z} - \alpha_1 (T_{1X} + H_{1X} T_{1z}) = 0; \tag{2.19}$$

$$\eta_2 V_{2z} - \eta_1 V_{1z} - \alpha_1 (T_{1Y} + H_{1Y} T_{1z}) = 0; \tag{2.20}$$

$$H_{1\tau} + U_1 H_{1X} + V_1 H_{1Y} = W_1; \tag{2.21}$$

$$T_1 = T_2;\ \kappa_1 T_{1z} = \kappa_2 T_{2z}; \tag{2.22}$$

$$z = H_2:\ -\eta_2 U_{2z} - \alpha_2 (T_{2X} + H_{2X} T_2) = 0; \tag{2.23}$$

$$-\eta_2 V_{2z} - \alpha_2 (T_{2Y} + H_{2Y} T_{2z}) = 0; \tag{2.24}$$

$$H_{2\tau} + U_2 H_{2X} + V_2 H_{2Y} = W_2; \tag{2.25}$$

$$\kappa_2 T_{2z} = -q(T_2 - T_g - Ax), \tag{2.26}$$

where subscripts z, X, Y and τ denote corresponding partial derivatives, U_j, V_j and W_j, $j = 1, 2$ are the leading-order terms in the expansions in powers of ϵ:

$$u_{xj} = U_j + \cdots,\ u_{yj} = V_j + \cdots,\ u_{zj} = \epsilon W_j + \cdots.$$

Solving the problem for the temperature fields, we find

$$T_1 = T_s - (T_s - T_g) D q \kappa_2 z + Ax, \tag{2.27}$$

$$T_2 = T_s - (T_s - T_g) D q [(\kappa_2 - \kappa_1) H_1 + \kappa_1 z] + Ax, \tag{2.28}$$

where

$$D = [\kappa_1 \kappa_2 + q(\kappa_2 - \kappa_1) H_1 + q \kappa_1 H_2]^{-1}. \tag{2.29}$$

Thus, in each layer the temperature gradient is inclined to the vertical direction. In the case of flat interfaces, the distribution of the temperature is piecewise linear. The x-components of the flow velocities generated by the thermocapillary stresses are determined by the following formulae:

$$U_1 = \frac{(T_s - T_g)\kappa_2}{\eta_1} [D(\alpha_1 q H_1 - \alpha_2 \kappa_1)]_X z - \frac{(\alpha_1 + \alpha_2) A}{\eta_1} z, \tag{2.30}$$

$$U_2 = \frac{(T_s - T_g)\kappa_2}{\eta_2} \left\{ -\alpha_2 \kappa_2 D_X z + \frac{H}{\eta_1} [D(\alpha_1 \eta_2 q H_1 - \alpha_2 (\eta_2 - \eta_1)\kappa_1)_X]_X \right\} - \left[\frac{\alpha_2}{\eta_2} (z - H_1) + \frac{\alpha_1 + \alpha_2}{\eta_1} H_1 \right] A. \tag{2.31}$$

The expressions for y-components of the flow velocities, V_1 and V_2, can be obtained from U_1 and U_2 by replacing X by Y. Solving the continuity equations with respect

to W_1 and W_2 with corresponding boundary conditions, we find that

$$W_1(X, Y, H_1) = -\int_0^{H_1} (U_{1X} + V_{1Y})\,\mathrm{d}z, \tag{2.32}$$

$$W_2(X, Y, H_2) = -\int_0^{H_1} (U_{1X} + V_{1Y})\,\mathrm{d}z + \int_{H_1}^{H_2} (U_{2X} + V_{2Y})\,\mathrm{d}z. \tag{2.33}$$

Using (2.32) and (2.33), we rewrite the kinematic conditions (2.21) and (2.25) in the following form:

$$H_{1\tau} + \left(\int_0^{H_1} U_1\,\mathrm{d}z\right)_X + \left(\int_0^{H_1} V_1\,\mathrm{d}z\right)_Y = 0, \tag{2.34}$$

$$H_{2\tau} + \left(\int_0^{H_1} U_1\,\mathrm{d}z + \int_{H_1}^{H_2} U_2\,\mathrm{d}z\right)_X + \left(\int_0^{H_1} V_1\,\mathrm{d}z + \int_{H_1}^{H_2} V_2\,\mathrm{d}z\right)_Y = 0. \tag{2.35}$$

Substituting expressions for flow velocities obtained above into (2.34) and (2.35), we arrive to a closed system of equations that governs the evolution of a heated two-layer film under the action of the thermocapillary effect:

$$H_{1\tau} + \nabla\cdot \boldsymbol{Q}_1^T = 0,\ \ H_{2\tau} + \nabla\cdot \boldsymbol{Q}_2^T = 0, \tag{2.36}$$

where

$$\boldsymbol{Q}_1^T = \frac{(T_s - T_g)\kappa_2}{2\eta_1} H_1^2 \nabla[D(q\alpha_1 H_1 - \alpha_2\kappa_1)] - \frac{(\alpha_1 + \alpha_2)A}{2\eta_1} H_1^2 \boldsymbol{e}_x, \tag{2.37}$$

$$\begin{aligned}\boldsymbol{Q}_2^T = {} & \frac{(T_s - T_g)}{2\eta_1\eta_2}\left\{H_2^2\nabla[(-\alpha_2\kappa_1\eta_1)D] + (2H_2 - H_1)H_1\nabla\left\{D[q\alpha_1\eta_2 H_1 - \alpha_2\kappa_1(\eta_2 - \eta_1)]\right\}\right\} \\ & - \left[\frac{\alpha_2 A}{2\eta_2}(H_2 - H_1)^2 + \frac{\alpha_1 + \alpha_2}{2\eta_1} A H_1(2H_2 - H_1)\right]\boldsymbol{e}_x,\end{aligned} \tag{2.38}$$

where $\boldsymbol{e}_x$ is the unit vector of the axis x.

2.2. *Flows in the presence of van der Waals forces*

In the framework of the continuum approach, the van der Waals forces manifest themselves as external normal stresses ('disjoining pressures') imposed on each interface (Israelachvili 1992). The disjoining pressures modify the dependences of the pressures P_1 and P_2 in each layer on the layer thicknesses H_1 and H_2 in the following way (Fisher & Golovin 2005):

$$P_1 = -\sigma_1\nabla^2 H_1 - \sigma_2\nabla^2 H_2 + W_1(H_1, H_2), \tag{2.39}$$

$$P_2 = -\sigma_2\nabla^2 H_2 + W_2(H_1, H_2), \tag{2.40}$$

where

$$W_1(H_1, H_2) = \frac{A_{sg} - A_{s2} - A_{g1}}{6\pi H_2^3} + \frac{A_{s2}}{6\pi H_1^3}, \tag{2.41}$$

$$W_2(H_1, H_2) = \frac{A_{sg} - A_{s2} - A_{g1}}{6\pi H_2^3} + \frac{A_{g1}}{6\pi(H_2 - H_1)^3}. \tag{2.42}$$

Here, A_{sg}, A_{s2} and A_{g1} are Hamaker constants characterizing the interactions between the solid substrate and the gas across the two layers, between the solid substrate and liquid 2 across liquid 1 and between the gas phase and liquid 1 across liquid 2, correspondingly.

It was shown earlier (Pototsky *et al.* 2005; Nepomnyashchy & Simanovsky 2006) that in the framework of the lubrication approximation, the influence of the surface tension and van der Waals forces on the dynamics of a non-isothermic two-layer thin film is described by additional flux terms in evolution equations:

$$H_{1\tau} + \nabla\cdot\left(\boldsymbol{Q}_1^T + \boldsymbol{Q}_1^{v\,\mathrm{d}W}\right) = 0,\ H_{2\tau} + \nabla\cdot\left(\boldsymbol{Q}_2^T + \boldsymbol{Q}_2^{v\,\mathrm{d}W}\right) = 0, \tag{2.43}$$

where

$$\boldsymbol{Q}_1^{v\,\mathrm{d}W} = \boldsymbol{Q}_1^0 = F_{11}\nabla P_1 + F_{12}\nabla P_2,\ \boldsymbol{Q}_2^{v\,\mathrm{d}W} = F_{21}\nabla P_1 + F_{22}\nabla P_2. \tag{2.44}$$

The pressures P_1 and P_2 are determined by expressions (2.39) and (2.40), and the mobility functions are

$$F_{11} = -\frac{1}{3\eta_1}H_1^3;\ F_{12} = -\frac{1}{2\eta_1}H_1^2(H_2 - H_1);\ F_{21} = \frac{1}{6\eta_1}H_1^3 - \frac{1}{2\eta_1}H_1^2H_2;$$
$$F_{22} = (H_2 - H_1)\left[H_1^2\left(\frac{1}{2\eta_1} - \frac{1}{3\eta_2}\right) + H_1H_2\left(-\frac{1}{\eta_1} + \frac{2}{3\eta_2}\right) - \frac{1}{3\eta_2}H_2^2\right].$$

Let us transform (2.43) to a non-dimensional form. The natural vertical length scale is the initial thickness of the lower layer H_1^0. At the present stage, we do not fix the horizontal length scale L^*. In Fisher & Golovin (2005), the characteristic scale

$$L^* = L_0^* = \left(H_1^0\right)^2\sqrt{6\pi\sigma_1^0/|A_{sg}|} \tag{2.45}$$

has been suggested, which is convenient for the analysis of the instability induced by intermolecular forces. We choose

$$\tau^* = \frac{\eta_1(L^*)^4}{\sigma_1^0\left(H_1^0\right)^3} \tag{2.46}$$

as a time scale and

$$p^* = \frac{\sigma_1^0H_1^0}{(L^*)^2} \tag{2.47}$$

as a pressure scale.

Equations (2.43) written in the non-dimensional form look as follows:

$$h_{1\tau} + \nabla\cdot\boldsymbol{q}_1 = 0,\ h_{2\tau} + \nabla\cdot\boldsymbol{q}_2 = 0, \tag{2.48}$$

$$\boldsymbol{q}_1 = f_{11}\nabla p_1 + f_{12}\nabla p_2 + \boldsymbol{q}_1^T,\ \boldsymbol{q}_2 = f_{21}\nabla p_1 + f_{22}\nabla p_2 + \boldsymbol{q}_2^T, \tag{2.49}$$

where $h_j = H_j/H_1^0$, $p_j = P_j/p^*$, $j = 1, 2$,

$$f_{11} = -\frac{1}{3}h_1^3,\ f_{12} = -\frac{1}{2}h_1^2(h_2 - h_1),$$
$$f_{21} = \frac{1}{6}h_1^3 - \frac{1}{2}h_1^2h_2,\ f_{22} = (h_2 - h_1)\left[h_1^2\left(\frac{1}{2} - \frac{\eta}{3}\right) + h_1h_2\left(-1 + \frac{2\eta}{3}\right) - \frac{\eta}{3}h_2^2\right].$$

We use the same notation τ and ∇ for new, non-dimensional, variables. Later on, we assume that the dependence of interfacial tensions on the temperature is relatively weak and can be neglected in the boundary conditions for *normal stresses* (but not in those for tangential stresses where it is the source of a thermocapillary motion). The contributions of disjoining pressures are included:

$$p_1 = -\nabla^2h_1 - \sigma\nabla^2h_2 + w_1(h_1, h_2), \tag{2.50}$$
$$p_2 = -\sigma\nabla^2h_2 + w_2(h_1, h_2), \tag{2.51}$$

$$w_1 = \frac{a_0 - a_1 - a_2}{h_2^3} + \frac{a_1}{h_1^3}, \tag{2.52}$$

$$w_2 = \frac{a_0 - a_1 - a_2}{h_2^3} + \frac{a_2}{(h_2 - h_1)^3}. \tag{2.53}$$

The non-dimensional expressions for the fluxes generated by the thermocapillary effect are

$$\boldsymbol{q}_1^T = \frac{M_\perp}{2} h_1^2 \nabla[d(Bi\, h_1 - \alpha\kappa)] - \frac{M_\parallel}{2}(1+\alpha) h_1^2 \boldsymbol{e}_x, \tag{2.54}$$

$$\boldsymbol{q}_2^T = \frac{M_\perp}{2}\left\{-h_2^2 \nabla(\mathrm{d}\eta\alpha\kappa) + (2h_2 - h_1)h_1 \nabla\{d[Bi\, h_1 - \alpha\kappa(1-\eta)]\}\right\}$$
$$- \frac{M_\parallel}{2}\left[\eta\alpha h_2^2 + (1 + \alpha - \eta\alpha)h_1(2h_2 - h_1)\right]\boldsymbol{e}_x. \tag{2.55}$$

Here

$$M_\perp = \frac{\alpha_1(T_s - T_g)}{\sigma_1^0}\left(\frac{L^*}{H_1^0}\right)^2, \tag{2.56}$$

$$M_\parallel = \frac{\alpha_1 A L^*}{\sigma_1^0}\left(\frac{L^*}{H_1^0}\right)^2 \tag{2.57}$$

are the modified transverse and longitudinal Marangoni numbers, correspondingly:

$$Bi = \frac{q H_1^0}{\kappa_2} \tag{2.58}$$

is the Biot number, and

$$d = [\kappa + Bi(1-\kappa)h_1 + Bi\,\kappa h_2]^{-1}, \tag{2.59}$$

$\eta = \eta_1/\eta_2$, $\kappa = \kappa_1/\kappa_2$, $\sigma = \sigma_2^0/\sigma_1^0$, $\alpha = \alpha_2/\alpha_1$,

$$a_0 = \mathrm{sign}(A_{sg})\left(\frac{L^*}{L_0^*}\right)^2,\ a_1 = \frac{A_{s2}}{|A_{sg}|}\left(\frac{L^*}{L_0^*}\right)^2,\ a_2 = \frac{A_{g1}}{|A_{sg}|}\left(\frac{L^*}{L_0^*}\right)^2. \tag{2.60}$$

If the scaling of the horizontal length is chosen as (2.45), then $|a_0| = 1$.

The system of (2.48) contains ten non-dimensional parameters: $M_\perp$, $M_\parallel$, Bi, σ, α, η, κ, a_0, a_1, and a_2.

Let us estimate the characteristic values of these parameters in the case $L^* = L_0^*$. Fisher & Golovin (2005) showed that for $H_1^0 \sim 100\,\mathrm{nm}$, the typical values of parameter L_0^* determined by (2.45) are between 20 and 200 μm. Thus, the ratio $\epsilon = H_1^0/L_0^*$ is between 5×10^{-4} and 5×10^{-3}, which justifies the longwave approach. The Marangoni numbers are determined by the intensity of the external heating. The assumption that the surface tension coefficients are linear functions of the temperature is reasonable when $\alpha_j|T_s - T_g| \ll \sigma_j^0$, $\alpha_j A L \ll \sigma_j^0$, $j = 1, 2$, where L is the characteristic size of the system in x-direction. Therefore, the modified Marangoni numbers should satisfy the conditions $M_\perp \ll \epsilon^{-2}$, $M_\parallel \ll \epsilon^{-2}(L^*/L)$. The Biot number characterizes the heat transfer at the free boundary. Generally, one can expect that this parameter is rather small in the case of a thin layer. However, the evaporation of film can significantly increase cooling at the liquid/gas interface and hence the effective Biot number (Colinet *et al.* 2003; Haut & Colinet 2005). Other six parameters are intrinsic characteristics of the multilayer system substrate/liquid 1/liquid 2/gas. Parameters α, η and σ are just ratios of physical parameters of the liquids, while a_0, a_1 and a_2

depend on the values of the Hamaker constants A_{sg}, A_{s2} and A_{g1}. The latter constants are determined by the dielectric permittivities of all the media as functions of the frequency (Lifshitz & Pitaevskii 1980; Israelachvili 1992), and they depend mainly on the zero-frequency dielectric constants and high-frequency refractive indices of the media (Israelachvili 1992; Pototsky *et al.* 2005).

3. Linear stability theory

3.1. *Dispersion relation*

Let us consider a parallel thermocapillary flow with plane interfaces located at $z = H_1^0$ and $z = H_2^0$. This flow corresponds to the *basic* solution of (2.48)

$$h_1 = 1,\ h_2 = h = 1 + a,$$

where $h = H_2^0/H_1^0$, $a = (H_2^0 - H_1^0)/H_1^0$.

In order to investigate the stability of the plane two-layer film, we substitute

$$h_1 = 1 + \tilde{h}_1,\ h_2 = 1 + a + \tilde{h}_2$$

into (2.48), and linearize them with respect to variables $\tilde{h}_1$, $\tilde{h}_2$.

The solutions of the linear problem can be written as

$$\tilde{h}_j(X, Y, \tau) = \bar{h}_j \mathrm{e}^{i\boldsymbol{k}\cdot\boldsymbol{R}+\lambda\tau},\ \ j = 1, 2, \tag{3.1}$$

where $\boldsymbol{R} = (X, Y)$, $\boldsymbol{k} = (k_x, k_y)$ is the wavevector, λ is the growth rate and $\bar{h}_j$, $j = 1, 2$ are constants. Substituting (3.1) into the linearized equations, we obtain a dispersion relation

$$\det(\boldsymbol{N} - \lambda \boldsymbol{I}) = 0, \tag{3.2}$$

which determines the eigenvalues $\lambda(\boldsymbol{k})$. Here $\boldsymbol{I}$ is the unit matrix, while matrix $\boldsymbol{N}$ can be presented in the following form:

$$\boldsymbol{N} = \boldsymbol{B} + \frac{M_\perp Bi k^2 \kappa}{2(\kappa + Bi + Bi\kappa a)^2}\boldsymbol{C} + \mathrm{i}k_x M_\parallel \boldsymbol{D}. \tag{3.3}$$

Matrix $\boldsymbol{B}$ presents the contribution of the van der Waals forces and surface tensions and has the following components:

$$B_{11} = -\frac{k^2}{3}(k^2 - 3a_1) - \frac{3k^2 a_2}{2a^3},$$

$$B_{12} = -k^2\left(\frac{1}{3} + \frac{a}{2}\right)\left[\sigma k^2 - \frac{3(a_0 - a_1 - a_2)}{(a+1)^4}\right] + \frac{3k^2 a_2}{2a^3},$$

$$B_{21} = -k^2\left(\frac{1}{3} + \frac{a}{2}\right)(k^2 - 3a_1) + \left[\frac{1}{2} - \frac{\eta}{3} + (a+1)\left(-1 + \frac{2\eta}{3}\right) - \frac{\eta}{3}(a+1)^2\right]\frac{3k^2 a_2}{a^3},$$

$$B_{22} = -k^2\left(\frac{1}{3} + \frac{a}{2}\right)\left[\sigma k^2 - \frac{3(a_0 - a_1 - a_2)}{(a+1)^4}\right]$$
$$+ ak^2\left[\frac{1}{2} - \frac{\eta}{3} + (a+1)\left(-1 + \frac{2\eta}{3}\right) - \frac{\eta}{3}(a+1)^2\right]$$
$$\times\left[\sigma k^2 - \frac{3(a_0 - a_1 - a_2)}{(a+1)^4} - \frac{3a_2}{a^4}\right].$$

The second and third terms in the right-hand side of (3.3) are caused by the thermocapillary effect. The elements of matrix $\boldsymbol{C}$ are as follows:

$$C_{11} = 1 + Bi(a+1) + \alpha(1-\kappa),$$
$$C_{12} = \alpha\kappa - Bi,$$
$$C_{21} = \eta\alpha a^2(1-\kappa) + (2a+1)[\alpha(1-\kappa) + 1 + Bi(a+1)],$$
$$C_{22} = \eta\alpha\kappa a^2 + (2a+1)(\alpha\kappa - Bi).$$

The elements of matrix $\boldsymbol{D}$ are as follows:
$D_{11} = 1 + \alpha$, $D_{12} = 0$, $D_{21} = (a/2)[1 + \alpha(1-\eta)]$, $D_{22} = 1 + \alpha(1+\eta a)$.

3.2. *Marangoni instability*

In this subsection, we consider sufficiently thick films where the influence of the van der Waals interactions is weak in comparison with the Marangoni effect.

First, let us neglect the intermolecular interactions ($a_j = 0$). In the longwave limit ($k^2 \ll 1$), we can also neglect the terms caused by the surface tensions, which are proportional to k^4 and hence are small with respect to Marangoni terms proportional to k^2. In that limit, the dispersion relation (3.2) becomes

$$\det[M_\perp \boldsymbol{E} k^2 + \mathrm{i}k_x M_\parallel \boldsymbol{D} - \lambda \boldsymbol{I}] = 0, \tag{3.4}$$

where

$$\boldsymbol{E} = \frac{Bi\kappa}{2(\kappa + Bi + Bi\kappa a)^2}\boldsymbol{C}. \tag{3.5}$$

Denote $m_\perp = M_\perp k^2$, $m_\parallel = M_\parallel k_x$, $\beta = m_\parallel / m_\perp$, $\lambda = m_\perp \Lambda$. The rescaled growth rate Λ satisfies the quadratic equation

$$\Lambda^2 - [\mathrm{tr}(\boldsymbol{E}) + \mathrm{i}\beta \mathrm{tr}(\boldsymbol{D})]\Lambda + \det(\boldsymbol{E}) + \mathrm{i}F\beta - \beta^2 D_{11} D_{22} = 0, \tag{3.6}$$

where $F = E_{11}D_{22} + E_{22}D_{11} - E_{12}D_{21}$.

Let us consider some particular cases.

3.2.1. *The case* $\beta = 0$

This case corresponds to a vertical temperature gradient ($M_\parallel = 0$) or longitudinal stripe orientation ($k_x = 0$). Let us emphasize that in this paper the longitudinal stripes are developed due to the *longwave* deformational instability and, hence, they are different from the *shortwave* longitudinal rolls studied by Demekhin, Kalliadasis & Velarde (2006). Recall the main results obtained by Nepomnyashchy & Simanovskii (2007). The growth rate

$$\Lambda = \Lambda_0 = \frac{Bi\kappa}{2(\kappa + Bi + Bi\kappa)^2}\sigma, \tag{3.7}$$

where σ satisfies the equation

$$\sigma^2 - \mathrm{tr}(\boldsymbol{C})\sigma + \det(\boldsymbol{C}) = 0, \tag{3.8}$$

$$\mathrm{tr}(\boldsymbol{C}) = 1 - Bi\,a + \alpha(1 + \eta\kappa a^2 + 2\kappa a), \tag{3.9}$$

$$\det(\boldsymbol{C}) = \eta\alpha a^2(\kappa + Bi + Bi\kappa a). \tag{3.10}$$

Obviously, $\det(\boldsymbol{C})$ is always positive, while $\mathrm{tr}(\boldsymbol{C})$ is positive when $Bi < Bi_c$ and negative when $Bi > Bi_c$; here

$$Bi_c = \frac{1 + \alpha(1 + \eta\kappa a^2 + 2\kappa a)}{a}. \tag{3.11}$$

It is clear from the expression

$$\sigma = \frac{1}{2}[\mathrm{tr}(\boldsymbol{C}) \pm \sqrt{(\mathrm{tr}(\boldsymbol{C}))^2 - 4\det(\boldsymbol{C})}] \tag{3.12}$$

that the real part of σ is positive for $Bi < Bi_c$ and negative for $Bi > Bi_c$. Therefore, the Marangoni instability is developed in the case when heating is from below ($T_s > T_g$, $M > 0$), when $Bi < Bi_c$, and for heating from above ($T_s < T_g$, $M < 0$), when $Bi > Bi_c$. Note that the critical Marangoni number for the longwave deformational instability is always equal to zero. This result, which is valid only when the gravity is neglected, is well known for both single-layer systems (Scriven & Sternling 1964; Goussis & Kelly 1991) and two-layer systems (Smith 1966). The instability is monotonic if $S = (\mathrm{tr}(\boldsymbol{C}))^2 - 4\det(\boldsymbol{C})$ is positive and oscillatory if S is negative. The expression for S can be presented in the following form:

$$S = a^2\{Bi^2 - 2[Bi_c + 2\eta\alpha(\kappa a + 1)] + Bi_c^2 - 4\eta\alpha\kappa\}. \tag{3.13}$$

One can see that S is negative (i.e. the instability is oscillatory) in the interval $Bi_- < Bi < Bi_+$, where

$$Bi_\pm = Bi_c + 2\eta\alpha(\kappa a + 1) \pm \sqrt{4\eta\alpha[Bi_c(\kappa a + 1) + \kappa + \eta\alpha(\kappa a + 1)^2]}, \tag{3.14}$$

and positive (i.e. the instability is monotonic) otherwise. Note that because the term

$$Bi_c^2 - 4\eta\alpha\kappa = [(1 - a\sqrt{\eta\alpha\kappa})^2 + \alpha(1 + 2\kappa a)][(1 + a\sqrt{\eta\alpha\kappa})^2 + \alpha(1 + 2\kappa a)]$$

in the expression for S is positive, both $Bi_\pm$ are positive. Thus, for any two-layer film, both monotonic and oscillatory instabilities are possible, depending on the Biot number.

3.2.2. *The case of small β*

This case corresponds to a nearly vertical temperature gradient or a nearly longitudinal disturbance orientation.

Let us present the renormalized eigenvalue Λ, which satisfies (3.6), in the form

$$\Lambda = \Lambda_0 + \beta\Lambda_1 + \beta^2\Lambda_2 + \cdots. \tag{3.15}$$

In the zeroth order, we obtain the equation

$$\Lambda_0^2 - \mathrm{tr}(\boldsymbol{E})\Lambda_0 + \det(\boldsymbol{E}) = 0; \tag{3.16}$$

its solutions are determined by expressions (3.7) and (3.8) analysed in the previous subsection. As we have seen, both real and complex eigenvalues are possible.

In the first order, we find

$$2\Lambda_0\Lambda_1 - \Lambda_1\mathrm{tr}(\boldsymbol{E}) - \mathrm{i}\Lambda_0\mathrm{tr}(\boldsymbol{D}) + \mathrm{i}F = 0;$$

hence

$$\Lambda_1 = \mathrm{i}\frac{\Lambda_0\mathrm{tr}(\boldsymbol{D}) - F}{2\Lambda_0 - \mathrm{tr}(\boldsymbol{E})}. \tag{3.17}$$

If Λ_0 is real, the first-order correction Λ_1 is purely imaginary. Thus, the longitudinal component of the temperature gradient does not influence the threshold of the monotonic instability in the order $O(\beta)$. For imaginary Λ_0 (on the threshold of the oscillatory instability), the correction Λ_1 is complex. Note that the real part of Λ_1 depends on the sign of $\mathrm{Im}\Lambda_0$, i.e. the waves moving in opposite directions grow differently. In other words, the oscillatory neutral curve is splitted into two curves.

Similarly, the second-order correction Λ_2 can be calculated as

$$\Lambda_2 = \frac{-\Lambda_1^2 + \mathrm{i}\Lambda_1 \mathrm{tr}(\boldsymbol{D}) + D_{11}D_{22}}{2\Lambda_0 - \mathrm{tr}(\boldsymbol{E})}. \tag{3.18}$$

Note that it is purely real for a monotonic mode (when Λ_0 is real and Λ_1 is imaginary).

3.2.3. *The case of large* β

This case corresponds to a strong inclination of the temperature gradient and a disturbance orientation not close to a longitudinal one. The solution of (3.6) can be written as

$$\Lambda = \Lambda_{-1}\beta + \Lambda_0 + \cdots. \tag{3.19}$$

For Λ_{-1}, we obtain the following quadratic equation:

$$\Lambda_{-1}^2 - \mathrm{i}\Lambda_{-1}\mathrm{tr}(\boldsymbol{D}) - D_{11}D_{22} = 0. \tag{3.20}$$

We find that the roots are

$$\Lambda_{-1}^+ = \mathrm{i}D_{11},\ \Lambda_{-1}^- = \mathrm{i}D_{22}, \tag{3.21}$$

thus the corresponding terms in the expansion (3.19) are purely imaginary and do not influence the stability. Note that the frequencies of the disturbances

$$\omega^\pm = -\mathrm{Im}\lambda^\pm = -m_\perp \mathrm{Im}\Lambda^\pm = -m_\parallel \mathrm{Im}\Lambda_{-1}^\pm,$$

hence

$$\omega^+ = -M_\parallel D_{11}k_x,\ \omega^- = -M_\parallel D_{22}k_x. \tag{3.22}$$

Thus, each mode of disturbances corresponds to a wave which propagates in the x-direction with a phase velocity which depends only on the number of the mode (+ or −) but is independent of the wavenumber (in the longwave limit). This phase velocity is proportional to the applied longitudinal temperature gradient.

The term Λ_0 is obtained from the relation

$$2\Lambda_0\Lambda_{-1} - \Lambda_{-1}\mathrm{tr}(\boldsymbol{E}) - \mathrm{i}\Lambda_0\mathrm{tr}(\boldsymbol{D}) + \mathrm{i}F = 0,$$

hence

$$\Lambda_0^+ = \frac{D_{11}\mathrm{tr}(\boldsymbol{E}) - F}{D_{11} - D_{22}},\ \Lambda_0^- = \frac{D_{22}\mathrm{tr}(\boldsymbol{E}) - F}{D_{22} - D_{11}}$$

are real.

Therefore, the growth rates

$$\mathrm{Re}\lambda^\pm = M_\perp k^2 \Lambda_0^\pm + o(1), \tag{3.23}$$

i.e. they do not depend on the orientation of the wavevector and on the longitudinal Marangoni number $M_\parallel$ (though the elements of matrix $\boldsymbol{D}$, which is related to the longitudinal temperature gradient, are significant).

We come to the conclusion that on the linear stage of the instability development, any longwave disturbances move in the x-direction and grow or decay (on a slower time scale) independently on the orientation of their wavevectors with the rate proportional to the transverse temperature gradient. In the limit $\beta \to \infty$ (purely horizontal temperature gradient), expressions (3.22) are exact (in the framework of the lubrication approximation used here, and in the absence of the van der Waals forces and the interfacial tensions).

Thus, we arrive at the following paradoxical situation. The longitudinal component of the temperature gradient is the only factor that violates the rotational symmetry

of the problem. However, when this component is sufficiently large, the isotropy of the problem is partially restored (the real part of the growth rate depends only on k^2 and does not depend on k_x in the leading order, while the imaginary part keeps its dependence on k_x), except the region of nearly longitudinal structures that have small β even for large $M_\parallel$.

Note that in the case of a thick layer, where shortwave rather than longwave instabilities take place, the growth rate depends essentially on the direction of the wavevector, except the case $M_\parallel \ll M_\perp$ (see, e.g. Nepomnyashchy *et al.* 2001; Shklyaev & Nepomnyashchy 2004).

3.2.4. *Numerical analysis of the dispersion relation*

The 'isotropization' of the real part of the growth rate (i.e. its independence on the direction of the wavevector) takes place also in the framework of the full dispersion relation (3.2).

We have calculated the dependence of the real part of the growth rate $\mathrm{Re}\lambda$ for the most unstable mode on the wavenumber (k_x, k_y) for a model system with the following values of parameters: $\eta = 1.2$, $\kappa = 1$, $\alpha = 1$, $a = 1.5$. The parameters characterizing the intermolecular interactions are chosen very small: $a_0 = 0.01$, $a_1 = -0.004$, $a_2 = -0.001$ (that means that $L^* = 0.1L_0^*$, see (2.60)). The characteristic values of the Biot number, (3.11) and (3.14), are $Bi_c = 5.13$, $Bi_- = 1.01$, $Bi_+ = 21.25$. For a fixed direction of the wavevector, determined by the angle $\varphi = \tan^{-1}(k_y/k_x)$, we have found the maximum growth rate

$$(\mathrm{Re}\lambda)_m(\varphi) = \max_k(\mathrm{Re}\lambda)(k\cos\varphi, k\sin\varphi).$$

As the first example, let us consider the case $Bi = 0.1$, $M_\perp = 1$, $\sigma = 0.8$. According to formulae presented in § 3.2.1, the instability at $M_\parallel = 0$ (and hence also in the case $M_\parallel \neq 0$, $\varphi = \pi/2$) is monotonic. The results of the computations are shown in figure 2. The value $(\mathrm{Re}\lambda)_m(\pm\pi/2)$ does not depend on $M_\parallel$. For relatively small $M_\parallel$, the maximum growth rate depends significantly on the orientation of the wavevector (line 1). With the growth of $M_\parallel$, a long 'plateau' is developed (lines 2 and 3): the maximum growth rate is nearly constant and increases rapidly when φ approaches $\pm\pi/2$. Note that $(\mathrm{Re}\lambda)_m(0) < (\mathrm{Re}\lambda)_m(\pi/2)$, i.e. the disturbance with a longitudinal orientation grows faster than any other disturbance. The dependences of the wavenumber $k_m(\varphi)$ corresponding to the maximum growth rate are similar.

As the second example, we present results of the computations carried out for $Bi = 10$, $M_\perp = -1$, $\sigma = 1.6$. The instability for $\varphi = \pi/2$ is oscillatory. As in the previous case, a 'plateau' is developed for sufficiently large $M_\parallel$, but this time $(\mathrm{Re}\lambda)_m(0) > (\mathrm{Re}\lambda)_m(\pi/2)$, i.e. the disturbance with a longitudinal orientation grows slower than the transverse one (see figure 3).

3.3. *The van der Waals instability*

Let us now consider the case of an ultra-thin film, where the influence of intermolecular forces is crucial. We adopt scaling (2.45). Recall that in the case of a one-layer film, the influence of the intermolecular forces is determined by a single Hamaker constant, and the dependence of the interaction energy between the gas phase and the substrate on the thickness of the layer is monotonic. Depending on the sign of the Hamaker constant, the film is either stable or unstable. In the unstable case, the development of the van der Waals instability leads to the film rupture, if it is not stopped by a repulsive interaction of another physical nature (e.g. by electrostatic interaction or steric repulsion).

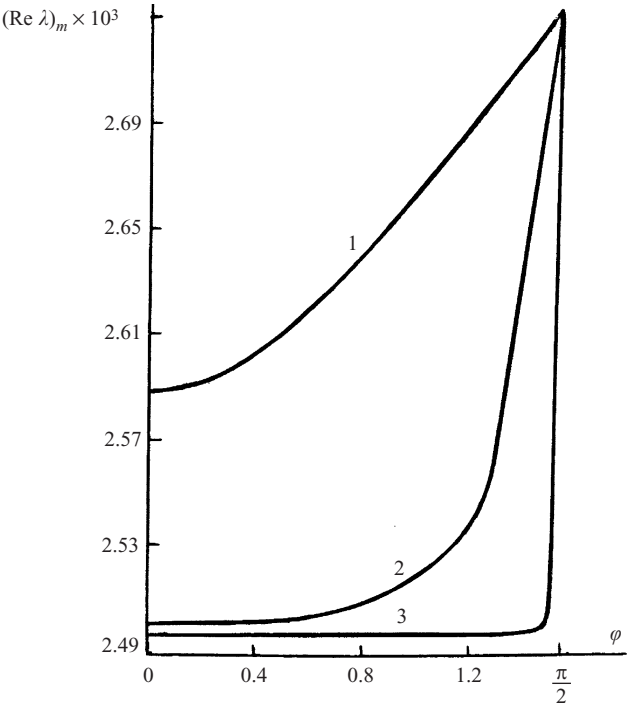

FIGURE 2. Dependence of the maximum growth rate $(\mathrm{Re}\lambda)_m$ on the angle φ for $M_{\parallel} = 0.01$ (line 1), $M_{\parallel} = 0.05$ (line 2) and $M_{\parallel} = 0.5$ (line 3). Other parameters are given in the text.

In the case of a two-layer film, the problem is characterized by three non-dimensional Hamaker constants a_0, a_1 and a_2 that characterize the interaction between the solid substrate and the gas phase across the two liquid layers, between the solid substrate and an infinite layer of liquid 2 across liquid 1, and between the gas and an infinite layer of liquid 1 across liquid 2, correspondingly (see Fisher & Golovin 2005). If $a_1 > 0$ or $a_2 > 0$, the effective interactions between corresponding adjacent interfaces are attractive, and they lead to a rupture of the bottom or top layer, correspondingly. A more interesting situation takes place when $a_1 < 0$, $a_2 < 0$, but $a_0 - a_1 - a_2 > 0$, i.e. the effective interaction between the liquid 2/gas interface and the liquid 1/substrate interface is attractive, while the effective interaction between adjacent interface is repulsive, one can expect that a van der Waals instability will develop, but it will not lead to the rupture of the layers (Fisher & Golovin 2005). Instead of rupture, one will observe a certain kind of 'spinodal decomposition' of the film into localized droplets and a thin 'precursor' film (Fisher & Golovin 2005; Nepomnyashchy & Simanovskii 2006).

In the present paper, we consider solely the latter case. The analysis is performed for the following set of parameters: $a_0 = 1$, $a_1 = -0.4$, $a_2 = -0.1$, $\eta = 1.2$, $\sigma = 0.8$, which corresponds to a model system formerly considered by Fisher & Golovin (2005). In this subsection, we investigate the film decomposition in the presence of Marangoni stresses. As in the previous subsection, other relevant parameters will be fixed as follows: $\kappa = 1$, $\alpha = 1$, $a = 1.5$.

In the absence of a transverse heating ($M_{\perp} = 0$), the Biot number is irrelevant. The effect of 'isotropization', similar to that discussed in the previous subsection, is also

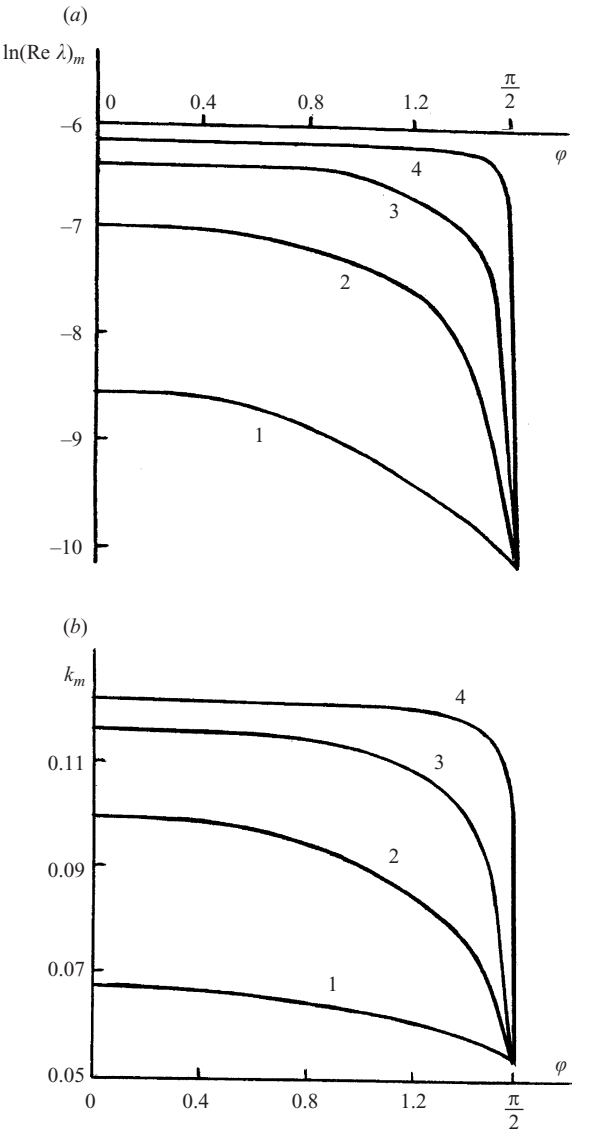

FIGURE 3. Dependences of (a) the maximum growth rate $(\mathrm{Re}\lambda)_m$ and (b) the corresponding wavenumber k_m on the angle φ for $M_\parallel = 0.001$ (line 1), $M_\parallel = 0.01$ (line 2), $M_\parallel = 0.05$ (line 3) and $M_\parallel = 0.5$ (line 4). Other parameters are given in the text.

observed in the case when the instability is caused by the action of the van der Waals forces, rather than by the action of the transverse temperature gradient. This effect is illustrated in figure 4.

Similar dependences of the growth rate on the orientation of the wavevector are observed in the cases when the instability is generated by a joint action of the van der Waals forces and the thermocapillary effect, for both ways of heating, from below (figure 5) and from above.

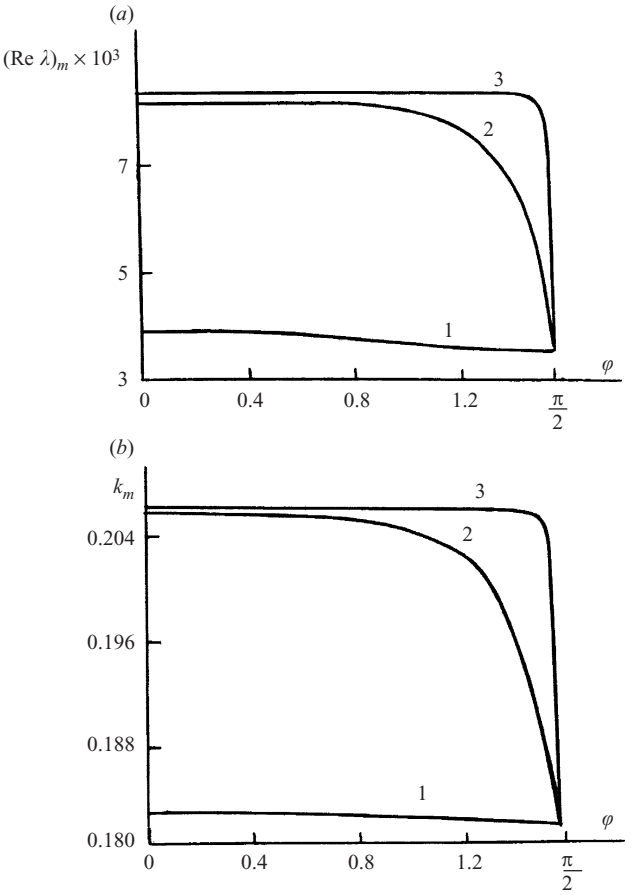

FIGURE 4. Dependences of (a) the maximum growth rate $(\mathrm{Re}\lambda)_m$ and (b) the corresponding wavenumber k_m on the angle φ for $M_\parallel = 0.01$ (line 1), $M_\parallel = 0.35$ (line 2) and $M_\parallel = 5$ (line 3). Other parameters are given in the text.

4. Nonlinear simulations

4.1. *Methodology*

The investigation of the film evolution under the joint action of the thermocapillary stresses and intermolecular forces governed by full nonlinear equations (2.48)–(2.55) has been fulfilled by means of nonlinear simulations.

The oscillatory linear instability, described in the previous section, is the origin of Hopf bifurcations that generate solutions in the form of spatially periodic travelling waves (generally, propagating in an oblique direction), standing waves and oscillatory patterns. The simplest kind of solutions, travelling waves, can be obtained by solving nonlinear ordinary differential equations (see, e.g. Thiele & Knobloch 2004).

However, it should be taken into account that the problem under consideration is subject to a *longwave instability*, i.e. the interval of instability is $0 < k < k_m$ (for a definite direction of the wavevector). Therefore, the spatially periodic solutions with the wavenumber k_m are always unstable with respect to the disturbances with $k < k_m$ near the bifurcation point. The instability of spatially periodic solutions typically leads either to a coarsening process (like in the case of the Cahn–Hilliard

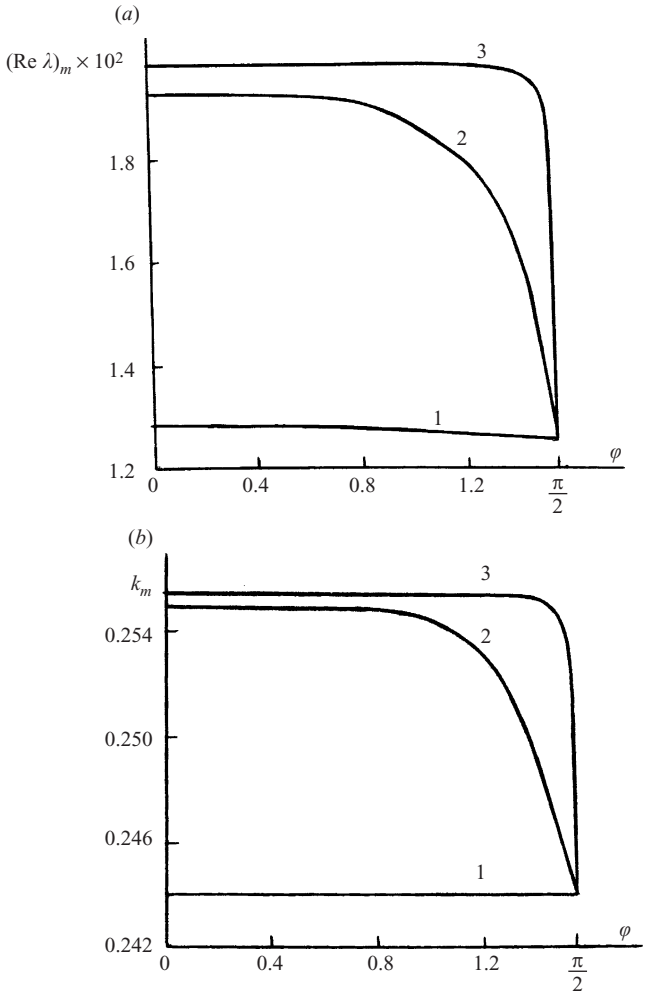

FIGURE 5. Dependences of (a) the maximum growth rate ($\mathrm{Re}\lambda)_m$ and (b) the corresponding wavenumber k_m on the angle φ for $M_{\parallel} = 0.01$ (line 1), $M_{\parallel} = 0.35$ (line 2) and $M_{\parallel} = 5$ (line 3). $M_{\perp} = 1$; $Bi = 0.1$; other parameters are given in the text.

equation) or to the development of a spatio-temporal chaos (like in the case of the Kuramoto–Sivashinsky equation). Under some conditions, stable spatially periodic travelling waves are also observed (see Golovin *et al.* 2001). Thus, in the case of a longwave instability, the computation of a bifurcation diagram for spatially periodic solutions is of no use without a simultaneous investigation of their stability with respect to disturbances with arbitrary spatial periods.

In the present paper, we overcome that difficulty in the following way. We consider the temporal evolution of the system with definite (typically random) initial conditions, and observe the behaviour of the system for large values of time. This approach allows us to obtain regimes of motion far more complicated than travelling waves. In the case when a travelling wave is observed as a final state, its stability is guaranteed.

It should be noted that this approach ignores unstable solutions of the problem. Therefore it does not allow us to obtain the full bifurcation diagram and hence

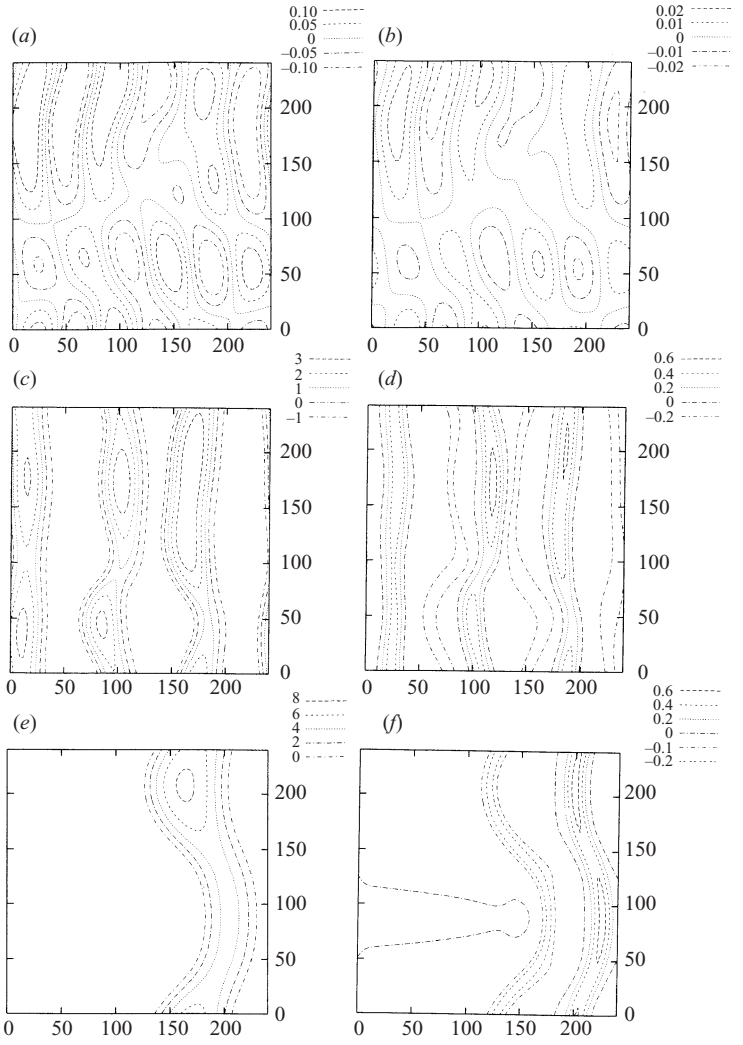

FIGURE 6. Isolines of $\tilde{h}_2(X, Y, \tau)$ (the left column) and $\tilde{h}_1(X, Y, \tau)$ (the right column); X is the abscissa, Y is the ordinate; (*a*), (*b*) $\tau = 10\,000$; (*c*), (*d*) $\tau = 20\,000$; (*e*), (*f*) $\tau = 120\,000$. Parameters are given in the text.

to determine the nature of bifurcations, leading to the transitions between different stable motions.

Evolution equations (2.48) have been discretized by central differences for spatial derivatives and solved using an explicit scheme. Periodic boundary conditions have been applied on the boundaries of the computational region. Initial conditions for h_j, $j = 1, 2$ have been chosen in such a way that the mean value of $h_1(X, Y, 0)$ was equal to 1 and the mean value of $h_2(X, Y, 0)$ was equal to h, where $h > 1$. Hence, our computations depend on the additional geometric parameter, $h = H_2^0/H_1^0$. Small random deviations of $h_j(X, Y, 0)$ from their mean values were imposed using a code creating pseudo-random numbers. The computations have been performed in the region 240×240 using the grid 400×400 for the following values of parameters: $\eta = 1.2$, $\kappa = 1$, $\alpha = 1$, $h = 2.5$.

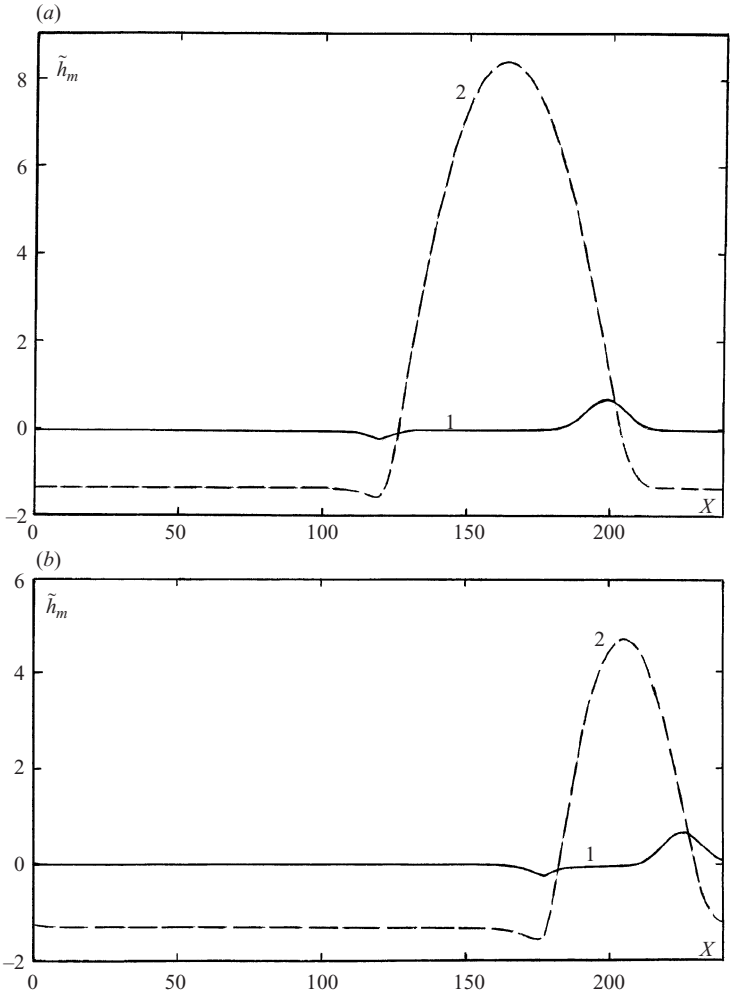

FIGURE 7. Cross-sections of $\tilde{h}_1(X, Y, \tau)$ (line 1) and $\tilde{h}_2(X, Y, \tau)$ (line 2); (*a*) $Y = 210$; (*b*) $Y = 91$; $\tau = 120\,000$. Parameters are given in the text.

4.2. *Nonlinear development of Marangoni instability*

4.2.1. *Stripe-like patterns*

In order to describe the influence of the longitudinal temperature gradient on the Marangoni-induced instability, we present results of the computations that have been carried out for the following set of parameters: $a_0 = 0.01$, $a_1 = -0.004$, $a_2 = -0.001$, $Bi = 10$, $M_\perp = -1$, $\sigma = 1.6$.

In the absence of the longitudinal heating ($M_\parallel = 0$), the problem is rotationally invariant. Simulations carried out in a computational region with spatially periodic boundary conditions reveal temporally non-periodic Marangoni oscillations (see figure 9 in the paper by Nepomnyashchy & Simanovskii 2007). The presence of sufficiently small $M_\parallel$ violates the isotropy of the problem: disturbances with wavevectors parallel to the direction of the thermocapillary flow have the maximum growth rate. This anisotropy leads to the development of more ordered structures than in the absence of a longitudinal heating. For $M_\parallel = 0.01$ (see line 2 in figure 3),

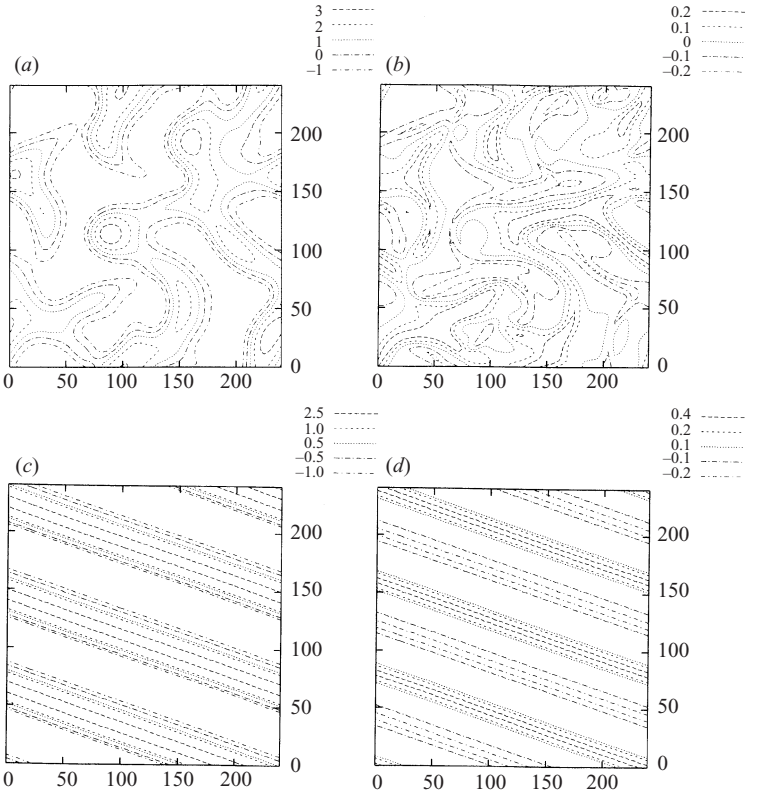

FIGURE 8. Isolines of $\tilde{h}_2(X, Y, \tau)$ (the left column) and (*b*) $\tilde{h}_1(X, Y, \tau)$ (the right column); X is the abscissa, Y is the ordinate; (*a*), (*b*) $\tau = 10\,000$; (*c*), (*d*) $\tau = 450\,000$. Parameters are given in the text.

the patterns that are developed during the stage of the linear growth are oriented across the direction of the base thermocapillary flow (see figure 6*a–b* where fields of $\tilde{h}_1(X, Y, \tau) = h_1(X, Y, \tau) - 1$ and $\tilde{h}_2(X, Y, \tau) = h_2(X, Y, \tau) - h$ are shown). The nonlinear development leads to the formation and coarsening of modulated transverse stripes (see figure 6*c–d*). Finally, the evolution of the system creates a strongly nonlinear travelling wave moving to the left with a constant velocity. No change of the wave shape is observed during a very long time (the computations have been carried out up to $\tau = 440\,000$). The free surface, $h_2(X, Y, \tau)$, contains a periodic system of droplets connected by 'necks' in the transverse direction (see figure 6*e*). The shape of the interface between the liquids, $h_1(X, Y, \tau)$, is more complex (figure 6*f*). It has a 'plateau' beneath the droplet and the neck, and elevations behind them. The longitudinal cross-sections $\tilde{h}_2(X, Y, \tau)$ and $\tilde{h}_1(X, Y, \tau)$ across the droplet ($Y = 210$) and the neck ($Y = 91$) are shown, correspondingly, in figures 7(*a*) and 7(*b*).

With the growth of $M_\parallel$, an 'isotropization' of the linear disturbances evolution takes place (see § 3.2.4). For $M_\parallel = 0.05$, the dependence of the maximum growth rate $(\mathrm{Re}\lambda)_m$ on the angle φ between the wavevector and the direction of the base flow has a 'plateau' in the region of sufficiently small φ (see line 3 in figure 3). Therefore, the disturbances with different orientations of the wavevector start to grow with nearly the same growth rate (see figure 8*a–b*). Finally, the nonlinear competition of disturbances leads to the development of a one-dimensional oblique non-modulated

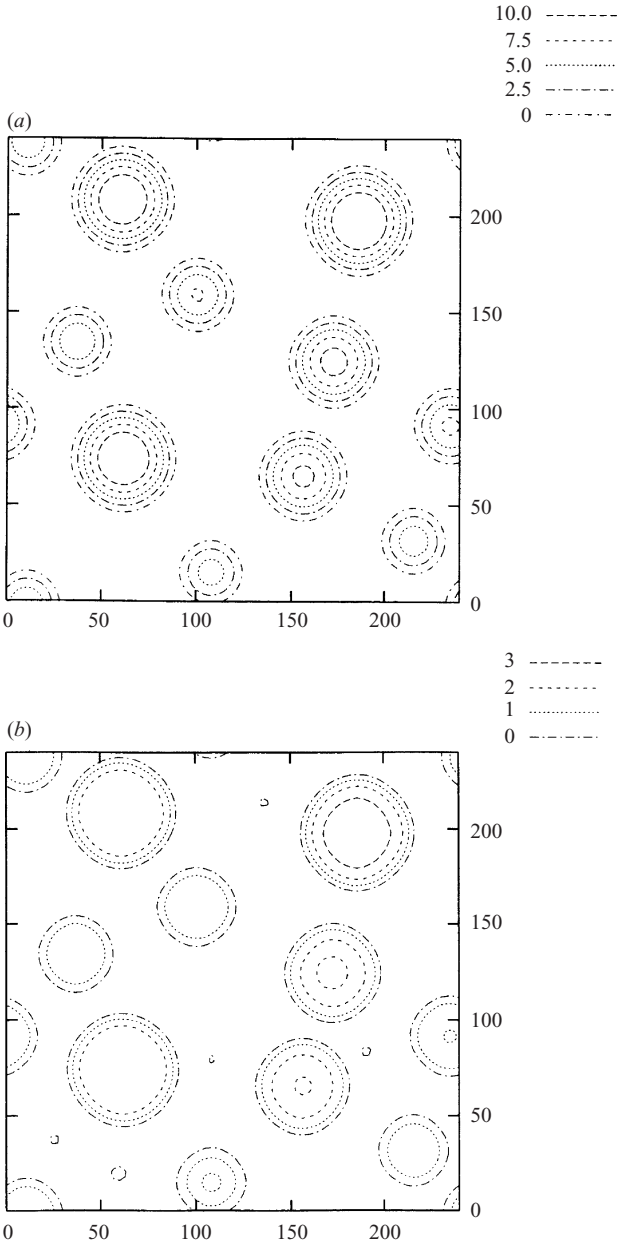

FIGURE 9. Isolines of (*a*) $\tilde{h}_2(X, Y, \tau)$ and (*b*) $\tilde{h}_1(X, Y, \tau)$; $M_\perp = 1$; $M_\parallel = 0$; $\sigma = 0.8$; $Bi = 0.1$; $\tau = 21\,300$.

travelling wave (see figure 8*c–d*)

$$h_j = h_j(\xi),\ \xi = \boldsymbol{X}\cdot\boldsymbol{n} + ct,\ \ j = 1, 2,$$

where $\boldsymbol{n}$ is a unit vector in the direction of the wavevector, c is the phase velocity of the wave, which moves in the negative direction with respect to axes X and Y. We have measured the phase velocity of the travelling wave by the comparison of its locations at different temporal snapshots, and have come to the conclusion that the

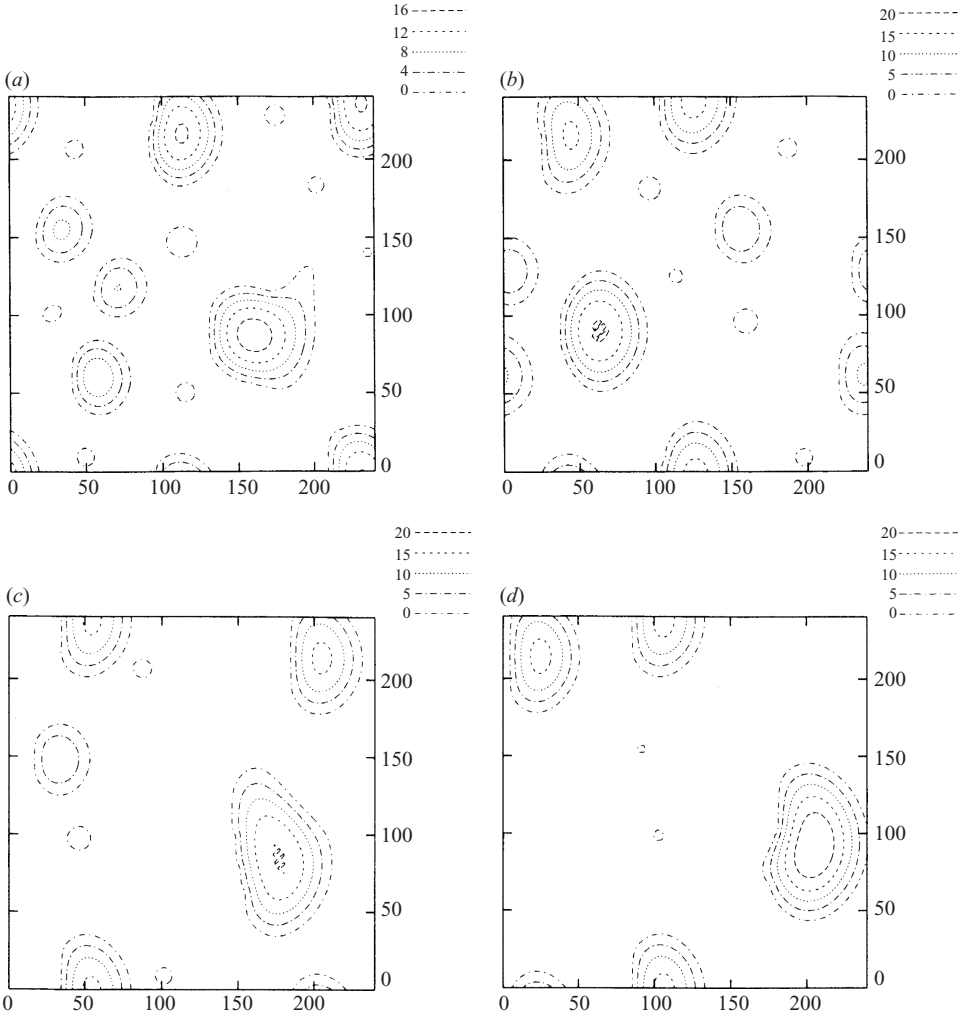

FIGURE 10. Isolines of $\tilde{h}_2(X, Y, \tau)$; X is the abscissa, Y is the ordinate; (*a*) $\tau = 11\,000$; (*b*) $\tau = 16\,000$; (*c*) $\tau = 21\,300$; (*d*) $\tau = 23\,000$; $M_\perp = 1$; $M_\parallel = 0.01$; $\sigma = 0.8$; $Bi = 0.1$.

phase velocity is constant. The nontrivial point is not the existence of such solutions, which is compatible with the predictions of the linear stability theory and with the symmetry properties of the system, but their stability. The shapes of deformations of both interfaces are similar to those discussed in the previous paragraph.

4.2.2. *Dynamics of droplets*

Another scenario of the nonlinear development of the Marangoni-induced instability in the absence of the longitudinal temperature gradient ($M_\parallel = 0$) leads to the decomposition of the film into droplets, which are subjected to a slow coarsening process. In figure 9, typical fields of $\tilde{h}_1(X, Y, \tau)$ and $\tilde{h}_2(X, Y, \tau)$ are shown for the system characterized by the following set of parameters: $a_0 = 0.01$, $a_1 = -0.004$, $a_2 = -0.001$, $Bi = 0.1$, $M_\perp = 1$, $\sigma = 0.8$ (predictions of the linear stability theory in this case are shown in figure 2). Note that the height of the droplets on the free surface

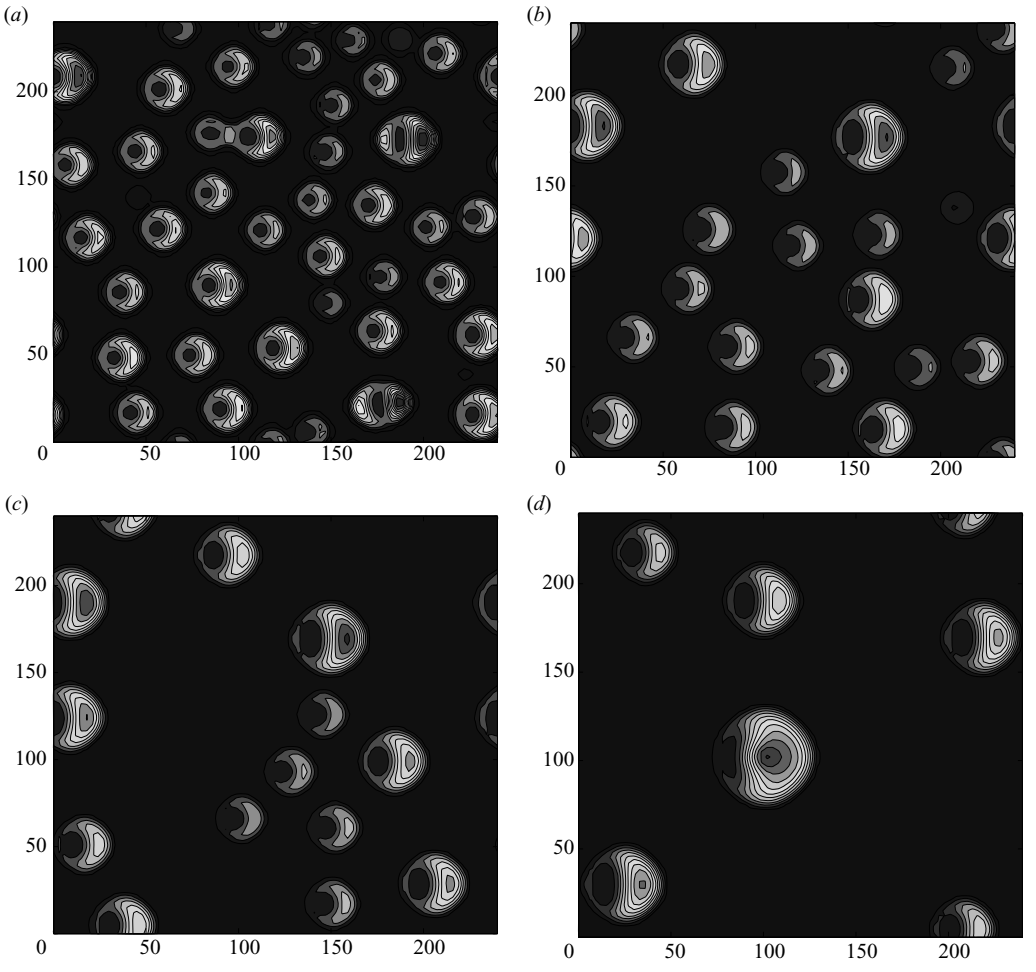

FIGURE 11. Isolines of $\tilde{h}_1(X, Y, \tau)$; X is the abscissa, Y is the ordinate; (a) $\tau = 2000$; (b) $\tau = 10\,000$; (c) $\tau = 20\,000$; (d) $\tau = 46\,000$. Parameters are given in the text.

is essentially larger than the deformation of the liquid–liquid interface beneath the droplets, but the locations of the structures at both interfaces coincide.

In the case $M_{\parallel} \neq 0$, the droplets move under the action of thermocapillary stresses in the direction opposite to that of the longitudinal temperature gradient. Two kinds of droplets, 'big' ones and 'small ones', are observed. The bigger is the droplet, the higher is its velocity (Nepomnyashchy & Simanovskii 2006). The motion of droplets gives rise to their coalescence and hence to an essentially faster coarsening process (see figure 10). The shape of the moving droplets is not round; the front side of a droplet is steeper than its back side.

4.3. *Nonlinear development of the van der Waals instability*

Now we discuss the influence of the inclined temperature gradient on the nonlinear development of the van der Waals instability. The content of this subsection has been partially presented at the Third International Topical Team Workshop on Two-Phase Systems for Ground and Space Applications (Bruxelles, Belgium, 10–12 September

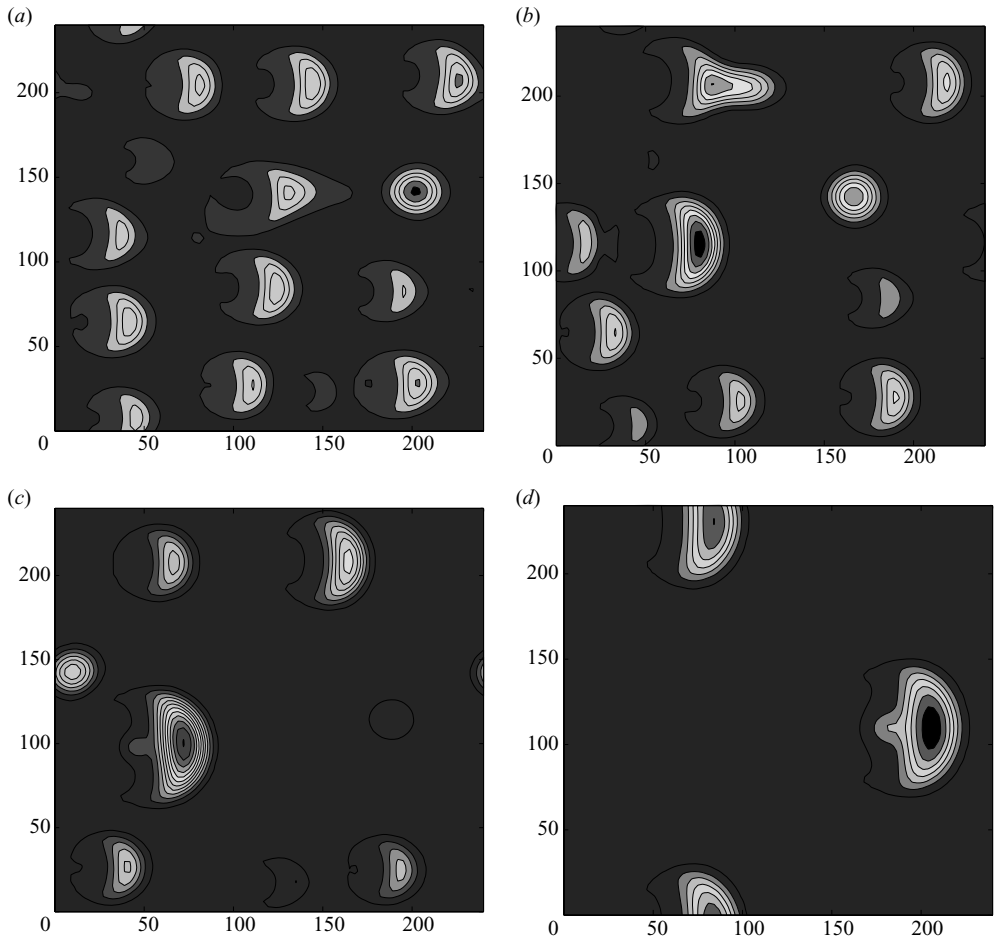

FIGURE 12. Isolines of $\tilde{h}_1(X, Y, \tau)$; X is the abscissa, Y is the ordinate; (*a*) $\tau = 10\,000$; (*b*) $\tau = 20\,000$; (*c*) $\tau = 26\,000$; (*d*) $\tau = 125\,000$. $M_\perp = 1$; $M_\parallel = 0.01$; other parameters are given in the text.

2008) and announced in the Proceedings of that workshop (Nepomnyashchy & Simanovskii 2008).

In contradistinction to the case of a purely transverse temperature gradient, where only coarsening droplets (or holes) are observed, the nonlinear dynamics in the case of an inclined temperature gradient is characterized by a large number of competing patterns. Below, we describe our observations.

4.3.1. *Droplets dynamics*

We describe the results of simulations done for system with the following set of parameters: $a_0 = 1$, $a_1 = -0.4$, $a_2 = -0.1$, $Bi = 0.1$, $\sigma = 0.8$.

First, let us recall results of simulations in the case $M_\parallel = 0$, $M_\perp > 0$ that have been carried out by Nepomnyashchy & Simanovskii (2007). The interfaces are decomposed into droplets that have a round shape, but the dependence of the liquid–liquid interface hight on the distance from the droplet centre becomes non-monotonic so that this interface resembles a 'volcano'. The droplets do not move; the coarsening takes place

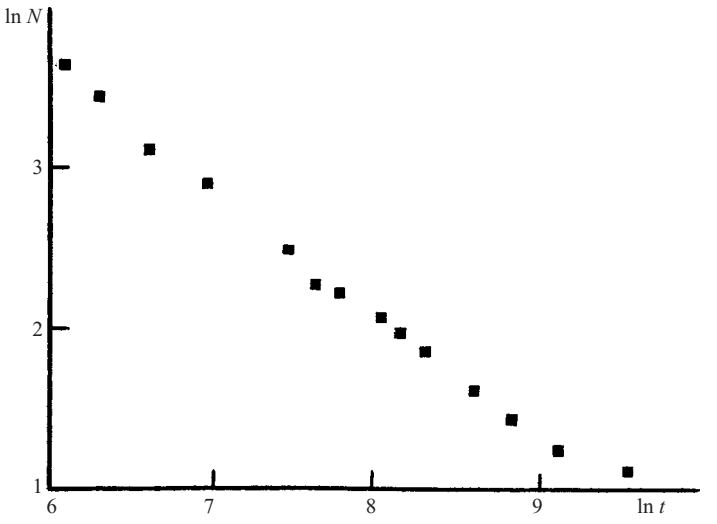

FIGURE 13. Dependence of the droplets number on time in the case $M_\perp = 0$, $M_\parallel = 0.05$, $h = 1.2$. Other parameters are given in the text.

due to the coalescence of large droplets caused by their growth and the disappearance of small droplets.

Let us now consider the nonlinear development of the van der Waals instability for $M_\parallel = 0.01$. As one can see in figure 4 (line 1) and figure 5 (line 1), the influence of such a small $M_\parallel$ on the real part of the linear growth rate and the critical wavenumber is negligible. We shall see, however, that the longitudinal component of the temperature gradient strongly influences the time evolution of structures on the nonlinear stage.

First, let us consider the case $M_\perp = 5$, $M_\parallel = 0.01$ ($M_\parallel / M_\perp = 0.002$). The coarsening of droplets is accelerated by their drift to the left due to the thermocapillary flow. The shape of the liquid–liquid interface beneath the droplets is strongly asymmetric: the crater-like depression is shifted to the left (front) part of the droplet, while in the right part of the droplet a high elevation is observed (see figure 11).

With the growth of the ratio $M_\parallel / M_\perp$, the free-surface droplet shapes become asymmetric; the asymmetry is especially strong for large droplets. The depressions in the front parts of the droplets become shallow (see figure 12).

Because of the thermocapillary flow, big droplets move faster than small ones; therefore, the droplets that have initially different values of coordinate X but close values of coordinate Y coalesce rapidly. A typical dependence of the droplets number on time is shown in figure 13. The characteristic time of coarsening in Y-direction is much higher. Finally, coarsening in Y-direction can be stopped: only few droplets survive which move in X-direction along separate 'running tracks'. Typically, the residual droplets have different sizes and move with different velocities.

Note that for a fixed value of $M_\parallel$, the characteristic wavenumber grows with the growth of $M_\perp$ (see figures 4 and 5). Therefore, the size of the droplets decreases, and their number increases when $M_\perp$ grows.

4.3.2. *Longitudinal stripes*

Let us now consider the nonlinear development of the van der Waals instability for $M_\parallel = 0.35$. As one can see in figure 5 (line 2), the growth rates of the disturbances with the wavevector inclinations in the interval $0 < \varphi < \pi/4$ have comparable values, while

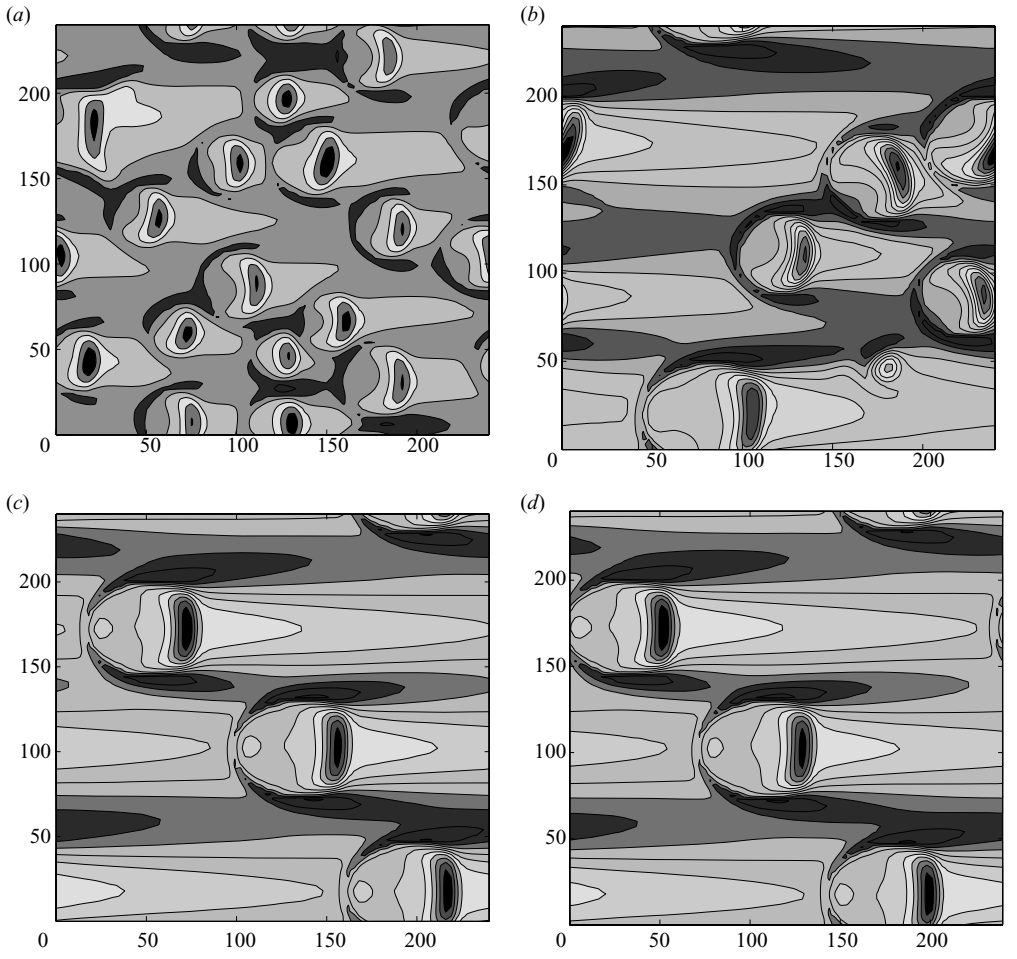

FIGURE 14. Isolines of $\tilde{h}_1(X, Y, \tau)$; X is the abscissa, Y is the ordinate; (*a*) $\tau = 2500$; (*b*) $\tau = 7500$; (*c*) $\tau = 60\,000$; (*d*) $\tau = 118\,000$. Parameters are given in the text.

the disturbances with larger inclination angles grow much slower. Therefore, in the early stage of the development, structures with transverse and inclined orientations are developed. However, further evolution of the system leads to a significant change of the structures: a system of longitudinal stripes is developed.

4.3.3. *Ordered structures*

In a certain region of parameters, we observed the formation of ordered structures that consist of equally sized droplets moving with equal velocities and located at equal distances from each other. An example of the formation of an ordered structure is shown in figure 14 ($M_\perp = -2.5$, $M_\parallel = 0.05$). In the initial stage of the coarsening a system of differently sized droplets is developed (figure 14*a–b*). Surprisingly, the evolution leads to the formation of three droplets with equal sizes (figure 14*c*) that finally become perfectly ordered and move with equal velocities (figure 14*d*).

Another example is shown in figures 15 and 16 ($M_\perp = -5$, $M_\parallel = 0.1$). The initial stage of the coarsening is quite usual (figures 15*a* and 16*a*). At the intermediate stage, one can observe a certain number of slightly asymmetric 'big' droplets, and some

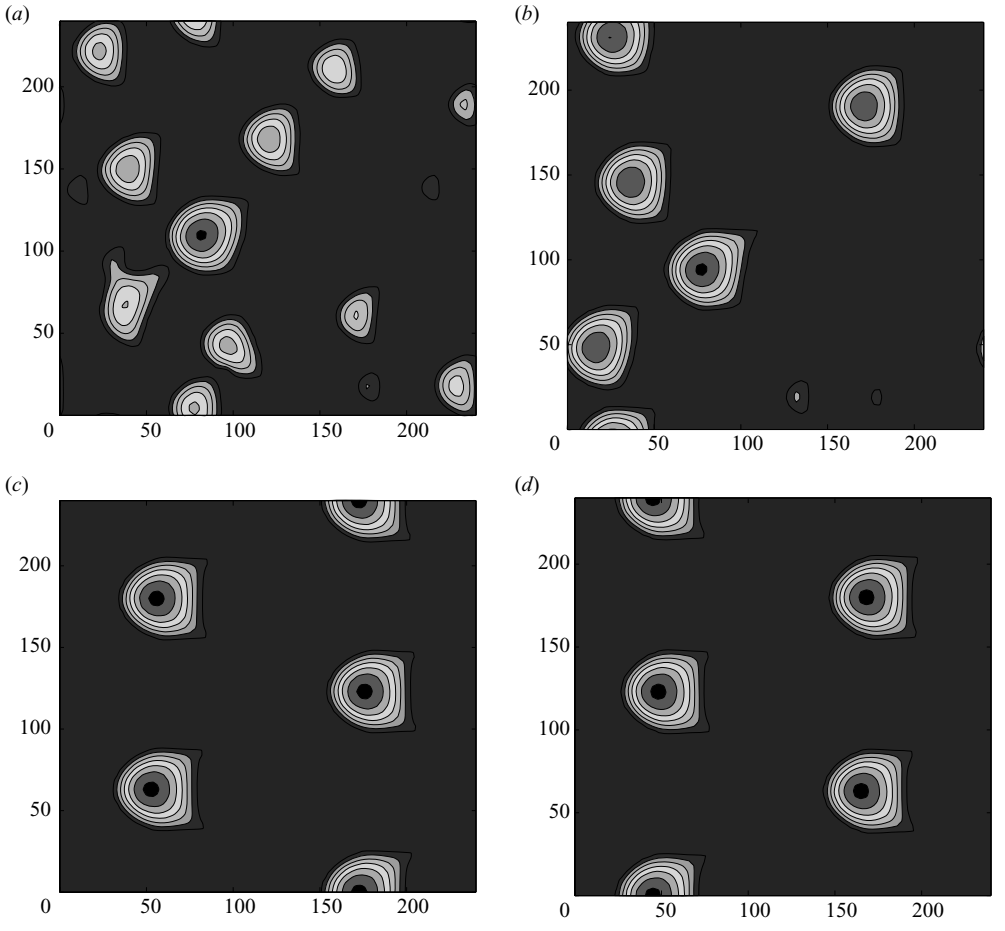

FIGURE 15. Isolines of $\tilde{h}_2(X, Y, \tau)$; X is the abscissa, Y is the ordinate; (*a*) $\tau = 2500$; (*b*) $\tau = 20\,000$; (*c*) $\tau = 120\,000$; (*d*) $\tau = 280\,000$. Parameters are given in the text.

droplets of small area, apparently created by a secondary instability of the liquid–liquid interface (splashes). It is remarkable that the deformation of the liquid–liquid interface caused by 'small' droplets is comparable with that caused by 'big' droplets (figure 16*b*), while the deformation of the free surface by 'small' droplets is almost negligible (figure 15*b*). Finally, the small droplets disappear, while the big droplets become perfectly ordered (figures 15*c* and 16*c*). The ordered system of droplets moves as the whole with a certain velocity to the left, and it does not evolve anymore (cf. figures 15*c*, 16*c* and figures 15*d*, 16*d*). The shapes of droplets are shown in figure 17. Note that the locations of droplets on both interfaces are correlated.

Let us emphasize that the ordered droplets system is not a result of a casual monodispersity of droplets due to a specific choice of initial conditions, but a result of a natural evolution of the systems to its stable configuration. The same ordered system of droplets has been obtained from different initial conditions. Note that the obtained structure reminds those observed in a falling viscous film (Saprykin, Demekhin & Kalliadasis 2005*a*, 2005*b*).

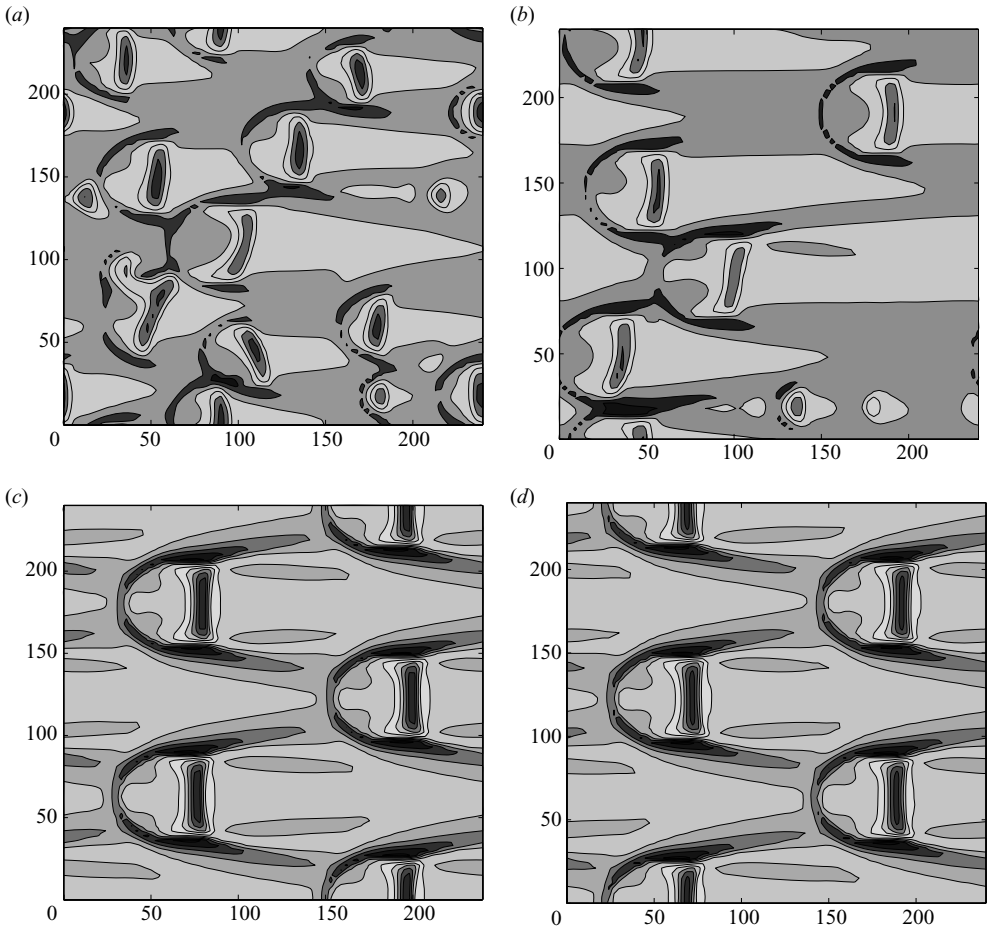

FIGURE 16. Isolines of $\tilde{h}_1(X, Y, \tau)$; X is the abscissa, Y is the ordinate; (*a*) $\tau = 2500$; (*b*) $\tau = 20\,000$; (*c*) $\tau = 120\,000$; (*d*) $\tau = 280\,000$. Parameters are given in the text.

4.3.4. *Disordered structures*

Outside the region of parameters corresponding to ordered structures, we observe a dynamical regime which is characterized by the coexistence of several 'immortal' big droplets and a number of small droplets that are ejected by big droplets, grow with time and finally coalesce with big droplets (see figures 18 and 19; $M_\perp = -5$, $M_\parallel = 0.11$). Note that a system of structures with essentially different sizes has been observed formerly in a viscous film flowing down an inclined plane (Indireshkumar & Frenkel 1997). As mentioned above, the hights of small droplets are comparable with hights of big droplets at the liquid–liquid interface, but they are relatively small at the free surface.

5. Conclusions

We have considered the evolution of a two-layer film under a joint action of thermocapillary effect and intermolecular forces in the case of an inclined temperature gradient. The governing equations have been derived in the lubrication approximation.

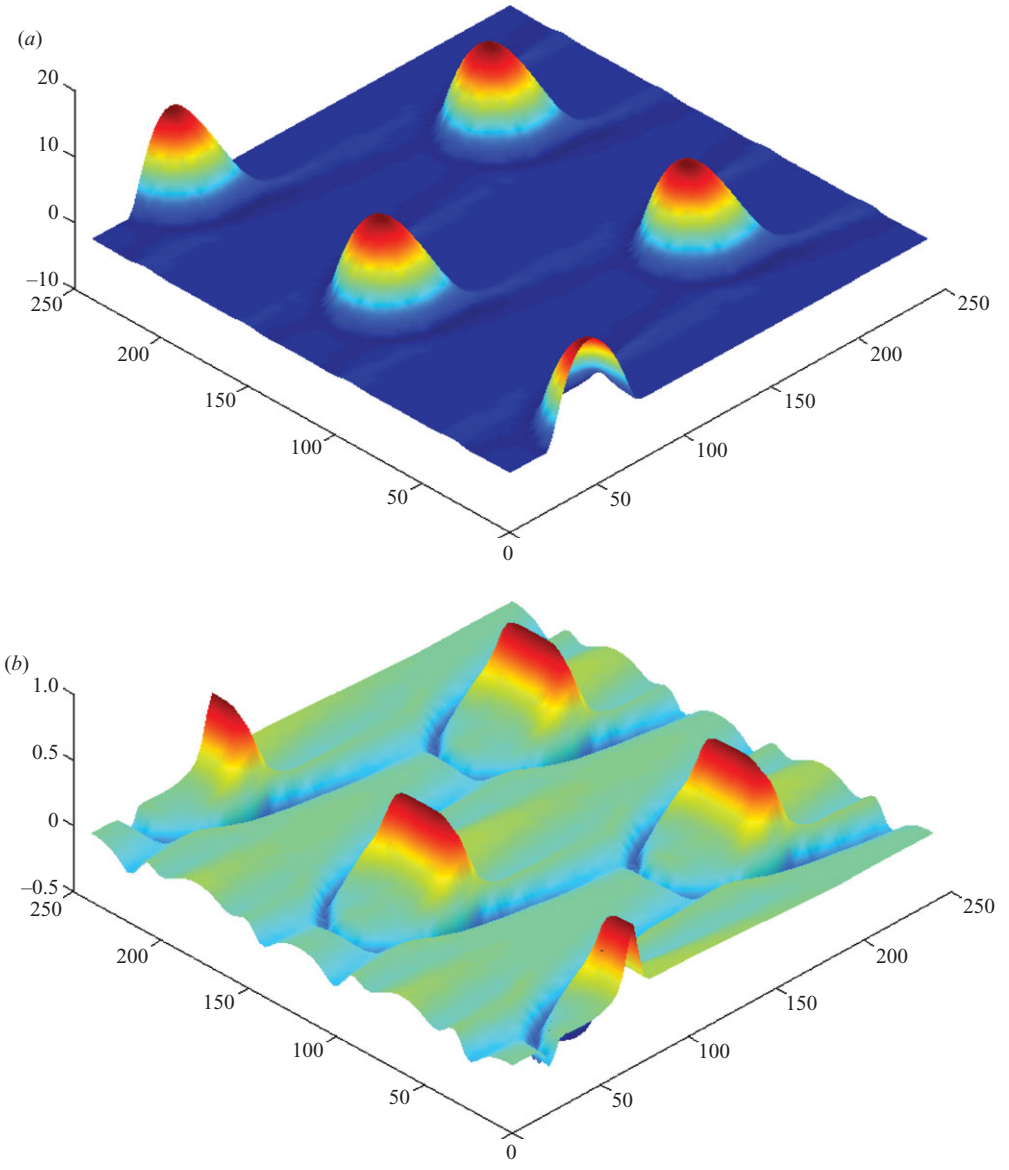

FIGURE 17. Shapes of interfaces at $\tau = 280\,000$; (*a*) $\tilde{h}_2(X, Y, \tau)$; (*b*) $\tilde{h}_1(X, Y, \tau)$; X is the abscissa, Y is the ordinate. Parameters are given in the text.

The development of instabilities is investigated in the framework of the linear stability theory and nonlinear simulations.

The analysis shows that the combined action of the transverse and longitudinal components of the temperature gradient can lead to novel phenomena that are not observed when only one of those components is present.

It is obvious that the appearance of the longitudinal component of the temperature gradient violates the rotational symmetry of the problem. It is unexpected, however, that for sufficiently large values of that component, the isotropy of the linear stability problem is partially restored (the real part of the linear growth rate is almost isotropic). Though this 'isotropization' is valid only on the initial (linear) stage of

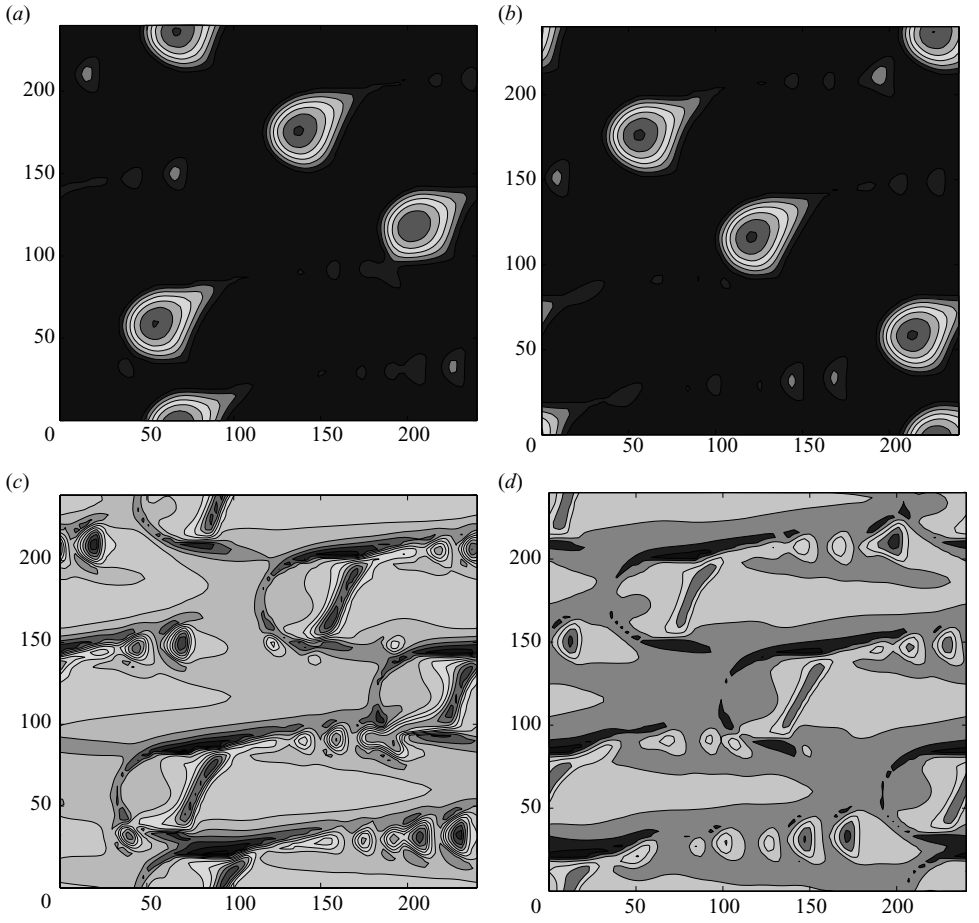

FIGURE 18. Isolines at $\tau = 60\,000$ ((*a*) $\tilde{h}_2(X, Y, \tau)$; (*c*) $\tilde{h}_1(X, Y, \tau)$) and $\tau = 60\,100$ ((*b*) $\tilde{h}_2(X, Y, \tau)$; (*d*) $\tilde{h}_1(X, Y, \tau)$); X is the abscissa, Y is the ordinate. Parameters are given in the text.

the disturbances growth, it influences the final nonlinear regime of the flow creating oblique waves instead of transverse waves in a certain region of parameters. In the regime of droplets, the longitudinal component of the temperature gradient is the origin of the droplets' motion and hence of their vigorous interaction. Depending on parameters, one observes a large number of novel motion regimes: ordered and disordered systems of droplets, 'splashes', modulated structures etc.

Finally, let us discuss the observability of the phenomena described above. The computations presented in § 4.1 correspond to $a_0 = (L^*/L_0^*)^2 = 0.01$. Using the estimates $H_1^0 \sim 100$ nm, $L_0^* \sim 100\,\mu$m, we come to the conclusion that the typical values of parameters $M_\perp \sim 1$ and $M_\parallel \sim 0.1$ correspond to the case $\alpha_1(T_s - T_g)/\sigma_1^0 \sim 10^{-4}$, $\alpha_1 A L_0^*/\sigma_1^0 \sim 10^{-4}$, i.e. the characteristic temperature differences in vertical and horizontal differences sufficient for the development of the abovementioned regimes are about 10^{-2} K. In our opinion, an appropriate system for the experimental investigation can be the system of two liquids, methanol/*n*-octane, that was used formerly in experiments on the Marangoni convection in relatively thick fluid layers (Nepomnyashchy *et al.* 2006).

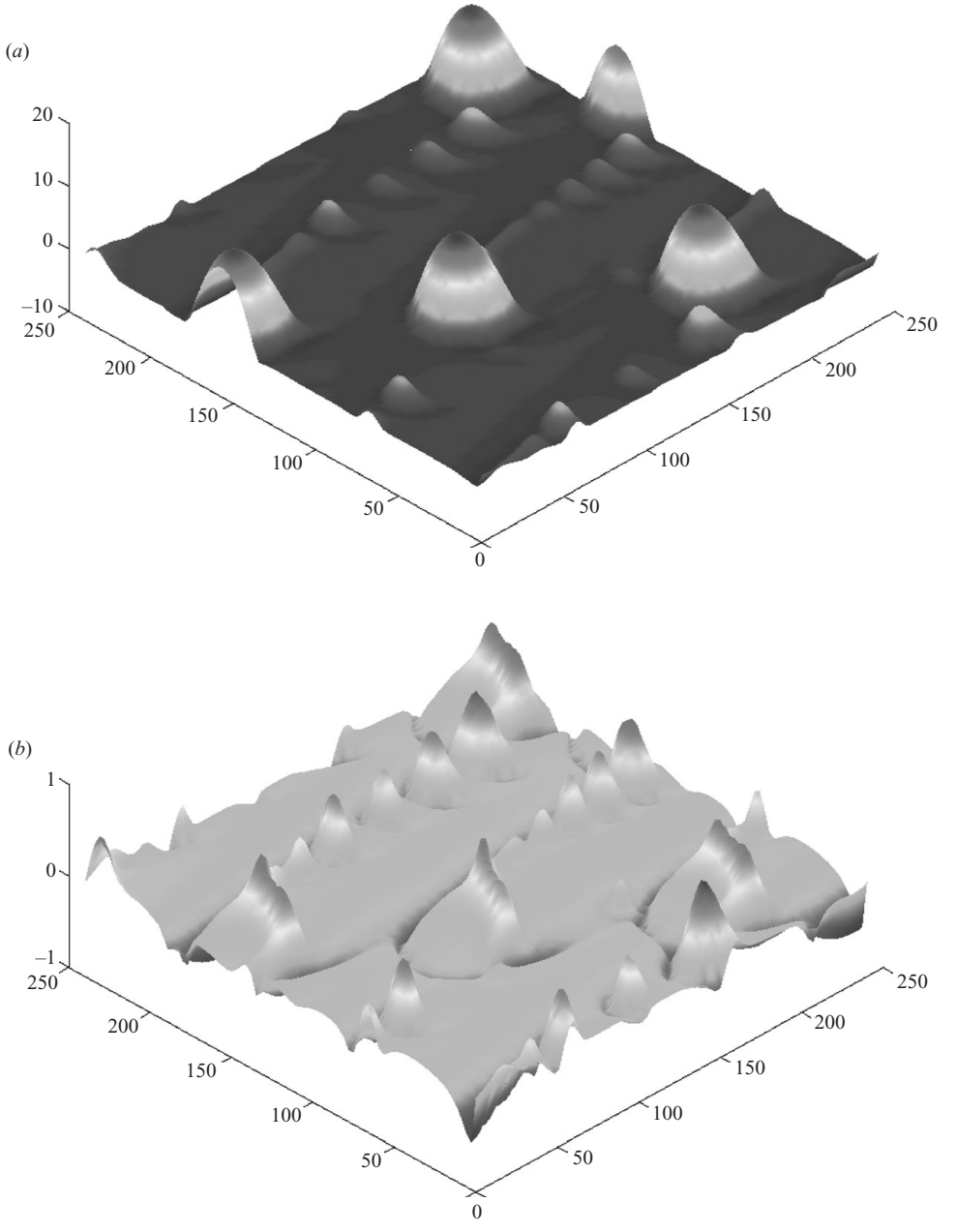

FIGURE 19. Shapes of interfaces at $\tau = 240\,000$; (*a*) $\tilde{h}_2(X, Y, \tau)$; (*b*) $\tilde{h}_1(X, Y, \tau)$. Parameters are given in the text.

The authors acknowledge the support of the Israel Ministry of Science (grant No. 3-3570). The research was partially supported by the European Union via the FP7 Marie Curie scheme (PITN-GA-2008-214919 (MULTIFLOW)).

REFERENCES

BANDYOPADHYAY, D., GULABANI, R. & SHARMA, A. 2005 Instability and dynamics of thin liquid bilayers. *Ind. Engng Chem. Res.* **44**, 1259.

Bandyopadhyay, D. & Sharma, A. 2006 Nonlinear instabilities and pathways of rupture in thin liquid bilayers. *J. Chem. Phys.* **125**, 054711.

Bandyopadhyay, D., Sharma, A. & Rastogi, C. 2008 Dewetting of the thin liquid bilayers on topologically patterned substrates: formation of microchannel and microdot arrays. *Langmuir* **24**, 14048.

Colinet, P., Joannes, L., Iorio, C. S., Haut, B., Bestehorn, M., Lebon, G. & Legros, J. C. 2003 Interfacial turbulence in evaporating liquids: theory and preliminary results of the ITEL-Master 9 sounding rocket experiment. *Adv. Space Res.* **32**, 119.

David, M. O., Reiter, G., Sitthai, T. & Schultz, J. 1998 Deformation of a glassy polymer film by long-range intermolecular forces. *Langmuir* **14**, 5667.

Davis, S. H. 1987 Thermocapillary instabilities. *Ann. Rev. Fluid Mech.* **19**, 403.

Demekhin, E. A., Kalliadasis, S. & Velarde, M. G. 2006 Suppressing falling film instabilities by Marangoni forces. *Phys. Fluids* **18**, 042111.

Faldi, F., Composto, R. J. & Winey, K. I. 1995 Unstable polimer bilayers. 1. Morphology of dewetting. *Langmuir* **11**, 4855.

Fisher, L. S. & Golovin, A. A. 2005 Nonlinear stability analysis of a two-layer thin liquid film: dewetting and autophobic behaviour. *J. Coll. Interf. Sci.* **291**, 515.

Golovin, A. A., Nepomnyashchy, A. A., Davis, S. H. & Zaks, M. A. 2001 Convective Cahn–Hilliard models: from coarsening to roughening. *Phys. Rev. Lett.* **85**, 1550.

Goussis, D. A. & Kelly, R. E. 1991 Surface wave and thermocapillary instabilities in a liquid film flow. *J. Fluid Mech.* **223**, 25.

Haut, B. & Colinet, P. 2005 Surface-tension-driven instabilities of a pure liquid layer evaporating into an inert gas. *J. Colloid Interf. Sci.* **285**, 296.

Indireshkumar, K. & Frenkel, A. L. 1997 Mutually penetrating motion of self-organized two-dimensional patterns of solitonlike structures. *Phys. Rev.* E **55**, 1174.

Israelachvili, J. N. 1992 *Intermolecular and Surface Forces*. Academic Press.

Joo, S. W. & Hsieh, K.-C. 2000 Interfacial instabilities in thin stratified viscous fluids under microgravity. *Fluid Dyn. Res.* **26**, 203.

Lambooy, P., Phelan, K. C., Haugg, O. & Krausch, G. 1996 Dewetting at the liquid-liquid interface. *Phys. Rev. Lett.* **76**, 1110.

Lenz, R. D. & Kumar, S. 2007*a* Competitive displacement of thin liquid films on chemically patterned substrates. *J. Fluid Mech.* **571**, 33.

Lenz, R. D. & Kumar, S. 2007*b* Instability of confined thin liquid film trilayers. *J. Coll. Interf. Sci.* **316**, 660.

Lifshitz, E. M. & Pitaevskii, L. P. 1980 *Statistical Physics*, Part 2. Pergamon.

Merkt, D., Pototsky, A., Bestehorn, M. & Thiele, U. 2005 Long-wave theory of bounded two-layer films with a free liquid-liquid interface: short- and long-time evolution. *Phys. Fluids* **17**, 064104.

Miladinova, S., Slavtchev, S., Lebon, G. & Legros J.-C. 2002 Long-wave instabilities of non-uniformly heated falling films. *J. Fluid Mech.* **453**, 153.

Morariu, M. D., Schaffer, E. & Steiner, U. 2003 Capillary instabilities by fluctuation induced forces. *Europ. Phys. J.* E **12**, 375.

Nepomnyashchy, A. A. & Simanovskii, I. B. 2006 Decomposition of a two-layer thin liquid film flowing under the action of Marangoni stresses. *Phys. Fluids* **18**, 112101.

Nepomnyashchy, A. A. & Simanovskii, I. B. 2007 Marangoni instability in ultrathin two-layer films. *Phys. Fluids* **19**, 122103.

Nepomnyashchy, A. A. & Simanovskii, I. B. 2008 Dynamics of non-isothermic ultra-thin two-layer films. In *Proceedings of the Third International Topical Team Workshop on Two-Phase Systems for Ground and Space Applications,* Bruxelles, Belgium; *Microgravity Sci. Technol.* **20** (3–4), 149–154.

Nepomnyashchy, A. A, Simanovskii, I. B. & Braverman, L. M. 2001 Stability of thermocapillary flows with inclined temperature gradient. *J. Fluid Mech.* **442**, 141.

Nepomnyashchy, A. A., Simanovskii, I. B. & Legros, J. C. 2006 *Interfacial Convection in Multilayer Systems*. Springer.

Oron, A., Davis, S. H. & Bankoff, S. G. 1997 Long-scale evolution of thin liquid films. *Rev. Mod. Phys.* **69**, 931.

Ospennikov, N. A. & Schwabe, D. 2004 Thermocapillary flow without return flow–linear flow. *Exp. Fluids* **36**, 938.

Pan, Q., Winey, K. I., Hu, H. H. & Composto, R. J. 1997 Unstable polimer bilayers. 2. The effect of film thickness. *Langmuir* **13**, 1758.

Pototsky, A., Bestehorn, M., Merkt, D. & Thiele, U. 2004 Alternative pathways of dewetting for a thin liquid two-layer film. *Phys. Rev.* E **70**, 025201.

Pototsky, A., Bestehorn, M., Merkt, D. & Thiele, U. 2005 Morphology changes in the evolution of liquid two-layer films. *J. Chem. Phys.* **122**, 224711.

Pototsky, A., Bestehorn, M., Merkt, D. & Thiele, U. 2006 Evolution of interface patterns of three-dimensional two-layer liquid films. *Europhys. Lett.* **74**, 665.

Renger, C., Muller-Buschbaum, P., Stamm, M. & Hinrichsen, G. 2000 Investigation and retardation of the dewetting on top of highly viscous amorphous substrates. *Macromolecules* **33**, 8388.

Saprykin, S., Demekhin, E. & Kalliadasis, S. 2005*a* Self-organization of two-dimensional waves in an active dispersive-dissipative nonlinear medium. *Phys. Rev. Let.* **94**, 224101.

Saprykin, S., Demekhin, E. & Kalliadasis, S. 2005*b* Two-dimensional wave dynamics in thin films. II. Formation of lattices of interacting stationary solitary pulses. *Phys. Fluids* **17**, 117106.

Scriven, L. E. & Sternling, C. V. 1964 On cellular convection driven by surface-tension gradients: effect of mean surface tension and surface viscosity. *J. Fluid Mech.* **19**, 321.

Sferrazza, M., Heppenstall-Butler, M., Cubitt, R., Bucknall, D., Webster, J. & Jones, R. A. L. 1998 Interfacial instability driven by dispersive forces: the early stages of spinodal dewetting of a thin polymer film on a polymer substrate. *Phys. Rev. Let.* **81**, 5173.

Sferrazza, M., Xiao, C., Jones, R. A. L., Bucknall, D. G., Webster, J. & Penfold, J. 1997 Evidence for capillary waves at immiscible polymer/polymer interfaces. *Phys. Rev. Let.* **78**, 3693.

Shklyaev, O. E. & Nepomnyashchy, A. A. 2004 Thermocapillary flows under an inclined temperature gradient. *J. Fluid Mech.* **504**, 99.

Simanovskii, I. B. & Nepomnyashchy, A. A. 1993 *Convective Instabilities in Systems with Interface.* Gordon and Breach.

Simanovskii, I., Nepomnyashchy, A., Shevtsova, V., Colinet, P. & Legros, J. C. 2006 Nonlinear Marangoni convection with the inclined temperature gradient in multilayer systems. *Phys. Rev.* E **73**, 066310.

Smith, K. A. 1966 On convective instability induced by surface-tension gradients *J. Fluid Mech.* **24**, 401.

Thiele, U. & Knobloch, E. 2004 Thin liquid films on a slightly inclined heated plate *Physica* D **190**, 213.

Ueno, I., Kurosawa, T. & Kawamura, H. 2002 Thermocapillary convection in thin liquid layer with temperature gradient inclined to free surface, Heat Transfer 2002. In *Proceedings of the Twelfth International Heat Transfer Conference,* Grenoble, France, pp. 129–134.